Bulletin of Volcanology (2019) 81: 67
https://doi.org/10.1007/s00445-019-1324-7

RESEARCH ARTICLE

# Time-dependent Sr and Nd isotope variations during the evolution of the ultrapotassic Sabatini Volcanic District (Roman province, Central Italy)

Gianluca Sottili[1] · Ilenia Arienzo[2] · Francesca Castorina[1,3] · Mario Gaeta[1] · Biagio Giaccio[4] · Fabrizio Marra[5] · Danilo M. Palladino[1]

Received: 22 March 2019 / Accepted: 5 September 2019 / Published online: 7 November 2019


## Abstract

The Sabatini Volcanic District (SVD), active between 0.8 and 0.07 Ma, is a volcanic field in the Roman province (Central Italy) located along the Tyrrhenian margin of the Italian peninsula. In this volcanic region, high-K magmas originated from a metasomatised phlogopite-bearing peridotite mantle recording subduction-related fluids and/or melting processes. Here, we investigate magma evolution during the six main eruptive phases of the SVD by means of chemical and isotopic (Sr and Nd) analyses. Specifically, we analyzed clinopyroxene crystals from juvenile pumice and scoria clasts and lavas, from 40 major SVD eruptive units chronologically well constrained by $^{40}Ar/^{39}Ar$ dating. $^{87}Sr/^{86}Sr$ and $^{144}Nd/^{143}Nd$ ratios in SVD clinopyroxene range 0.7095–0.7115 and 0.51210-0.51214, respectively. The mean Sr and Nd isotope compositions of each eruptive phases show a gradual, long-term decrease over the entire SVD eruptive history. However, when considering the distinct temporal windows of the individual eruptive phases, a significant variability of the Sr-Nd isotope ratios emerges, thus highlighting a more complex, time-dependent geochemical trend for the erupted magmas, with respect to a previously described trend at the nearby Colli Albani Volcanic District (0.6–0.04 Ma). Geochemical features of clinopyroxene in lavas and juvenile pyroclasts suggest that magma differentiation occurred in an open system due to assimilation of siliciclastic sedimentary rocks. Moreover, a critical review of the available geochemical data, in light of $^{40}Ar/^{39}Ar$ ages, allows the recognition of the SVD as the source of widespread tephra markers recorded in the central Mediterranean area by previous works.

**Keywords** Sabatini Volcanic District · Roman province · Sr and Nd isotopes

Editorial responsibility: S. Self

**Electronic supplementary material** The online version of this article (https://doi.org/10.1007/s00445-019-1324-7) contains supplementary material, which is available to authorized users.

✉ Gianluca Sottili
gianluca.sottili@uniroma1.it

[1] Dipartimento di Scienze della Terra, Sapienza-Università di Roma, P.le A. Moro 5, 00185 Rome, Italy

[2] Istituto Nazionale di Geofisica e Vulcanologia, Osservatorio Vesuviano, Via Diocleziano 328, 80124 Naples, Italy

[3] Istituto di Geologia Ambientale e Geoingegneria (IGAG)-CNR, c/o Dipartimento di Scienze della Terra, Sapienza-Università di Roma, P.le A. Moro 5, 00185 Rome, Italy

[4] Istituto di Geologia Ambientale e Geoingegneria (IGAG)-CNR, Monterotondo, 00015 Rome, Italy

[5] Istituto Nazionale di Geofisica e Vulcanologia, Sezione Sismologia e Tettonofisica, Via di Vigna Murata 605, 00147 Rome, Italy

## Introduction

Reconstructing the magmatic evolution of potassic systems over long time scales requires an integrated approach based on classic stratigraphic methods and geochemical cross-correlations of age-constrained deposits to track the evolution of magma through time. The Roman province (Washington 1906) volcanic history is quite well constrained based on proximal and distal (lacustrine) products across Italy. However, some outstanding questions regarding the origin and evolution of potassic magmatism are still open. In this regard, the Sabatini Volcanic District (SVD; Fig. 1) represents an ideal case study to focus due to its wide variety of potassic rock types and eruptive styles. The SVD is a volcanic field part of the Roman province (Washington 1906; Peccerillo 2001; Conticelli et al. 2010) which developed during the Pleistocene along the Tyrrhenian Sea margin of the Italian peninsula. The high-K magmas erupted in the SVD have been

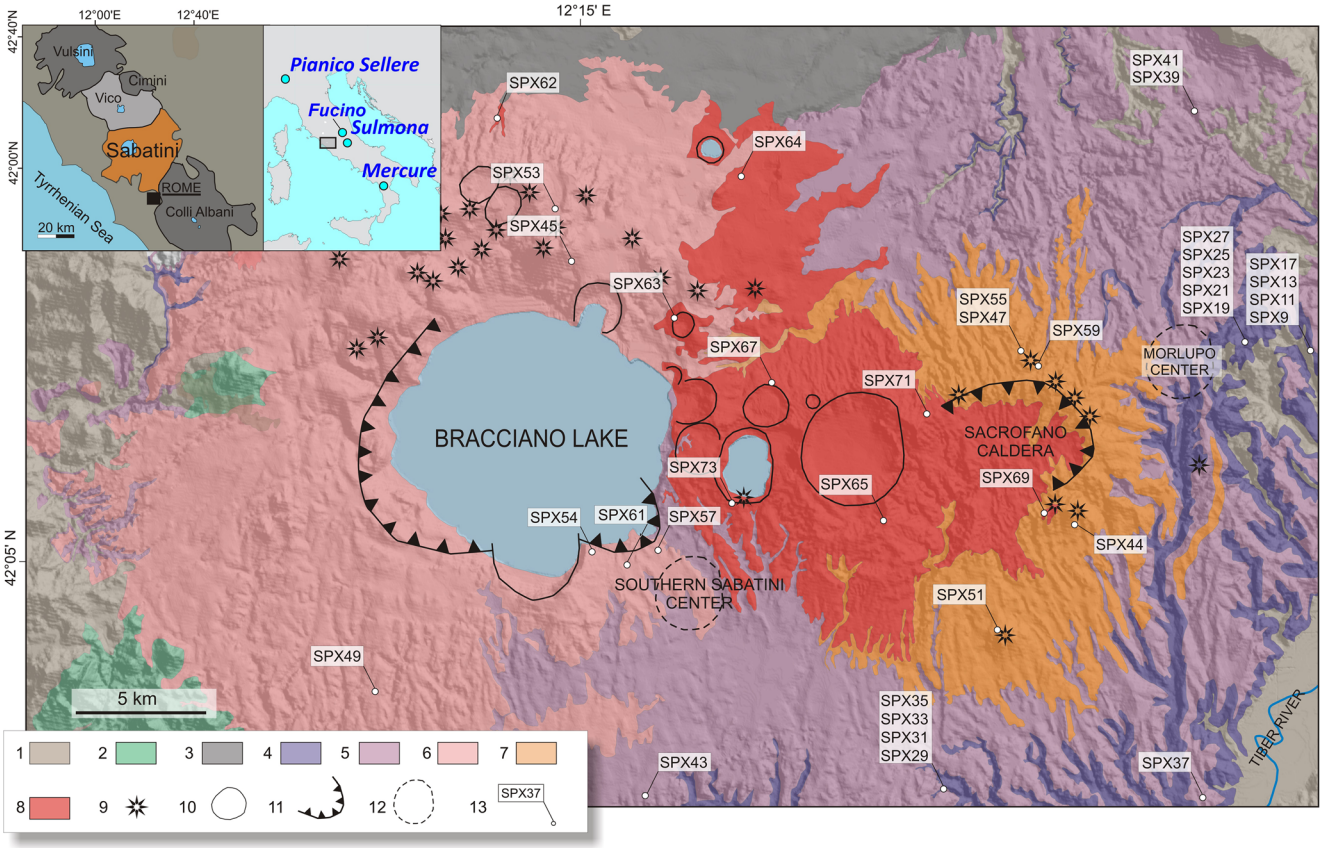


**Fig. 1** Simplified geologic map of the Sabatini Volcanic District (SVD), after Sottili et al. (2010a), showing the areal distributions of the main activity periods and the sampling locations for $^{87}Sr/^{86}Sr$ and $^{143}Nd/^{144}Nd$ determinations. Insets show the locations of the SVD and the other volcanic districts in the Roman province, central Italy. The locations of the tephrostratigraphic records of Mercure, Sulmona, and Pianico Sellere basins, possibly related to the SVD activity, are also reported (Roulleau et al. 2009; Giaccio et al. 2009, 2013a, 2014, 2015). Legend: 1—Sedimentary terrains; 2—M.ti Ceriti-Tolfetano-Manziate lava domes (Pliocene); 3—Vico Volcanic District (0.5–0.1 Ma); 4—Morlupo products (0.6–0.5 Ma); 5—Southern Sabatini products (0.5–0.4 Ma); 6—Bracciano Caldera products (0.3–0.2 Ma); 7—Sacrofano Caldera products (0.3–0.2 Ma); 8—SVD Late activity (< 0.15 Ma); 9—Scoria cones; 10—Maars; 11—Caldera rims; 12—Buried source areas; 13—$^{87}Sr/^{86}Sr$ sample locations. Coordinates of samples recovered in boreholes (SPX 1, SPX3, SPX5, and SPX7) are reported in Table 1

related to a metasomatized mantle source identified as a phlogopite-bearing peridotite recording subduction-related fluids and/or melting processes (Peccerillo 1985; Beccaluva et al. 1991; Conticelli and Peccerillo 1992; Peccerillo 1999; Conticelli et al. 2002). In particular, the subduction of carbonate-rich pelites has been proposed to play an important role in the origin of silica-undersaturated ultrapotassic rocks (kalsilite- and leucite-bearing) of the Roman province (Conticelli et al. 2015). Alternatively, a geodynamical model where vertical mixing across a slab window allowed the eruption of plume-type magmas in a subduction environment has been developed (Gasperini et al. 2002). This has been based on the contribution of isotope data (Sr, Nd, Hf, and Pb) from relatively undifferentiated basaltic lavas of Plio-Quaternary Italian volcanism, including two bulk samples from the SVD. However, the geochemical features of the Roman province magmas (i.e., high concentrations of LILE and LREE, associated with low concentrations of HFSE, and the high initial $^{87}Sr/^{86}Sr$ and low $^{143}Nd/^{144}Nd$ ratios) also suggest a combined effect of crystal fractionation and crustal assimilation during the evolution of the parental magmas (Hawkesworth and Vollmer 1979; Conticelli et al. 1997, 2002).

Detailed studies on individual Roman volcanoes (e.g., Conticelli and Peccerillo 1992; Conticelli et al. 1997; Perini et al. 2004, Gaeta et al. 2006; Boari et al. 2009) focused on discerning the geochemical fingerprints of the parental magma vs. those acquired during low-pressure processes. Based on petrological data, incompatible trace element abundances and isotope analyses on bulk lava rock types, Conticelli et al. (1997) defined two distinct, i.e., high-Ba and low-Ba, series in the SVD products, possibly related to the ascent of two different magma batches from the mantle source. However, this petrological study considered only effusive products, which represent a small fraction of the total erupted magma at the SVD.

The variations of $^{87}Sr/^{86}Sr$ in clinopyroxene from juvenile pyroclasts, in the frame of well-constrained

chronostratigraphic settings, allowed the reconstruction of the temporal changes of the primary magmas and their metasomatized mantle sources at other volcanoes of central Italy, including Colli Albani (Gaeta et al. 2006, 2016), Middle Valle Latina (Boari et al. 2009), Roccamonfina (Conticelli et al. 2009), and Monte Amiata (Conticelli et al. 2015; Laurenzi et al. 2015). More specifically, the isotopic and trace element heterogeneities through the whole Colli Albani eruptive history (0.6–0.04 Ma) have been ascribed to the evolution of a single metasomatized mantle source rather than to different mantle sources acting at the same time (Gaeta et al. 2006, 2016; Boari et al. 2009; Conticelli et al. 2015).

Here, we report on chemical and isotopic (Sr and Nd) compositions of clinopyroxene from SVD ultrapotassic rocks, including juvenile pyroclasts (pumice and scoria) and lava flows (40 eruptive units were sampled; Table 1), set within a well-constrained $^{40}Ar/^{39}Ar$ age frame. Using these data, we present a complete picture of the Sr and Nd isotopic variations through the whole SVD eruptive history, with implications for the magma source evolution.

## Volcanic history of the Sabatini Volcanic District

The SVD activity (0.8–0.07 Ma; Fig. 2) can be grouped into six main periods, characterized by volumetrically dominant explosive eruptions, ranging from hydromagmatic and Strombolian to Plinian and large pyroclastic flow forming events (VEI up to 4–5; erupted magma volumes up to tens of $km^3$ DRE), and subordinate effusive episodes (Karner et al. 2001; Sottili et al. 2004, 2010a; Marra et al. 2014, 2017, 2019). In order to maintain the greatest possible uniformity with previous literature, the $^{40}Ar/^{39}Ar$ ages reported in this paper (Table 1) are all calculated according to the age of 28.201 Ma for the Fish Canyon Tuff sanidine (Kuiper et al. 2008) and of 1.186 Ma for the Alder Creek sanidine (Jicha et al. 2016). However, differences with respect to other calibrations for the standard ages (Renne et al. 2011; Rivera et al. 2013) would be small and, in most cases, within the associated errors at 2 σ.

### Paleo-activity (810–610 ka)

The oldest outcropping products, attributed to a poorly known SVD Paleo-activity, consist of several tephra layers, sporadically intercalated within Late Lower-Early Middle Pleistocene fluvial deposits of the Paleo-Tiber River, dated between 808 ± 6 ka and 611 ± 6 ka (Karner and Renne 1998; Karner et al. 2001; Florindo et al. 2007). In particular, seven tephra layers, which represent the earliest evidence of volcanic activity in the Roman province (Marra and Florindo 2014), were recovered in five boreholes in the northern sector of the city of Rome (Florindo et al. 2007) and ascribed to three eruptive units (Marra et al. 2014) of uncertain source area.

### Morlupo activity (590–510 ka)

This second period of activity took place in the eastern sector of the SVD and can be divided into three main subphases (de Rita et al. 1993; Marra et al. 2014): early (~ 590 ka), middle (~ 550 ka), and late (~ 510 ka). Facies analyses, and isopach and isopleth maps, for the deposits of major explosive events consistently indicate a common vent area (Marra et al. 2014), corresponding to the Morlupo center (de Rita et al. 1993). Here, the main stratigraphic units and marker horizons are briefly described, as follows (from bottom to top):

- The Tufo Giallo di Castelnuovo di Porto (Tufo Giallo = yellow tuff; 589 ± 4 ka) is recognized discontinuously in the eastern sector of the SVD, where it is largely buried by younger SVD pyroclastic deposits in proximal and distal settings (Marra et al. 2014)
- The First Ash Fall Deposits (FAD; 589 ± 4 ka - 546 ± 3 ka), defined by Karner et al. (2001) in a relatively distal setting along the Tiber Valley (~ 20 km South of the source area), in proximal settings consist of a series of pumice fall units (FAD1, FAD2, and FAD3) locally separated by mature brown paleosoils
- The Tufo Giallo della Via Tiberina (546 ± 3 ka) groups a series of widespread pyroclastic flow deposits exposed in the eastern SVD sector, attributed to two main eruptive units (namely, the Lower and the Upper Tufo Giallo della Via Tiberina; Masotta et al. 2010; Marra et al. 2014), separated by a mature paleosoil, with an estimated total volume in the order of ~ 10 $km^3$ DRE (Marra et al. 2014). Noteworthy the Upper Unit is characterized by the occurrence of clinopyroxene-bearing granular enclaves (Marra et al. 2014)
- The Sella di Corno pumice fall, a ~ 25 cm pumice fall horizon found in an inter-Apennine distal setting (523 ± 10 ka, Gaeta et al. 2003), has been recognized in the eastern sector of the SVD, ~ 2 km SE from the inferred location of the Morlupo center (Marra et al. 2014)
- The Tufo Giallo di Prima Porta (516 ± 1 ka) was first described in the southern SVD area, along the Tiber Valley (Karner et al. 2001; Marra et al. 2017). In the eastern SVD sector, close to the Morlupo center, this unit rests on top of a mature, brown paleosoil and comprises a lower whitish pumice fall subunit (~ 3 m maximum thickness close to the Morlupo center), characterized by a stratified appearance due to multiple grading (Marra et al. 2014) and an upper subunit consisting of a massive or weakly stratified, 15–20-m-thick, pyroclastic flow deposit

**Table 1** $^{87}Sr/^{86}Sr$ and $^{143}Nd/^{144}Nd$ analyses of clinopyroxene and associated $^{40}Ar/^{39}Ar$, on Sabatini Volcanic District units. The external reproducibility 2σ, i.e. ± 0.000017 for Sr and ± 0.000010 for Nd, calculated according to Goldstein et al. (2003), represent the measurements errors (Fig. 6). For Sr measurements, the error is within the symbols. Ages are re-calculated from original publication according to the following references: 1—Karner et al. (2001); 2—Florindo et al. (2007); 3—Marra et al. (2014); 4—Gaeta et al. (2003); 5—Marra et al. (2017); 6—Marra et al. (2017); 7—Sottili et al. (2010a); 8—Pereira et al. (2017); 9—Nappi and Mattioli (2003); 10—Marra et al. (2019). All ages are calibrated for the Fish Canyon Tuff sanidine at 28.201 Ma (Kuiper et al. 2008) and Alder Creek sanidine at 1.186 Ma (Jicha et al. 2016), except those in italics for which the standard is not reported

| Samples | Unit | Abbreviation | $^{40}Ar/^{39}Ar$ age (ka) [ref.] | | Long. (E) | Lat. (N) | $^{87}Sr/^{86}Sr$ | $^{143}Nd/^{144}Nd$ |
|---|---|---|---|---|---|---|---|---|
| SPX1 | PT2b(S2) | | 808 ± 6 | [1] | 12° 31′ 04″ | 41° 55′ 14″ | 0.71128 | 0.51214 |
| SPX3 | PT-S14A | | 800 ± 11 | [2] | 12° 31′ 28″ | 41° 56′ 23″ | 0.71117 | 0.51213 |
| SPX5 | R95-16a | | 763 ± 8 | [1] | 12° 21′ 00″ | 41° 50′ 27″ | 0.71127 | 0.51213 |
| SPX7 | ING01bis | | 653 ± 4 | [1] | 12° 30′ 39″ | 41° 49′ 31″ | 0.71140 | 0.51213 |
| SPX9 | Tufo Giallo di Castelnuovo di Porto | TGCP | 589 ± 4 | [3] | 12°32′12″ | 42°09′03″ | 0.71144 | 0.51212 |
| SPX11 | First ash fall deposits | (FAD1) | ~ 589 ± 4 | [3] | 12°32′12″ | 42°09′03″ | 0.71143 | 0.51211 |
| SPX13 | First ash fall deposits | (FAD3) | 546 ± 5 | [3] | 12°32′12″ | 42°09′03″ | 0.71150 | 0.51211 |
| SPX17 | Lower Tufo Giallo Via Tiberina | LTGVT | – | | 12°32′12″ | 42°09′03″ | 0.71035 | 0.51211 |
| SPX19 | Upper Tufo Giallo Via Tiberina | UTGVT | 546 ± 3 | [1] | 12°30′25″ | 42°09′04″ | 0.71107 | 0.51211 |
| SPX21 | Sella di Corno Plinian Fall | SCP | 523 ± 10 | [4] | 12°30′25″ | 42°09′04″ | 0.71027 | 0.51211 |
| SPX23 | Tufo Giallo di Prima Porta | TGPP | 516 ± 1 | [5] | 12°30′25″ | 42°09′04″ | 0.71118 | 0.51211 |
| SPX25 | Grottarossa pyroclastic sequence | GRPS | 510 ± 4 | [5] | 12°30′25″ | 42°09′04″ | 0.71084 | 0.51210 |
| SPX27 | Fall A unit | Fall A | 498 ± 2 | [5] | 12°30′25″ | 42°09′04″ | 0.71143 | 0.51210 |
| SPX29 | Fall B unit | Fall B | 494 ± 14 | [6] | 12°30′25″ | 42°09′04″ | 0.71111 | 0.51210 |
| SPX31 | Fall C unit | Fall C | 461 ± 2 | [5] | 12°30′25″ | 42°09′04″ | 0.71042 | 0.51210 |
| SPX33 | Tufo Rosso a Scorie Nere | TRSN | 452 ± 2 | [1] | 12°30′25″ | 42°09′04″ | 0.71081 | 0.51210 |
| SPX35 | Fall E Unit | Fall E | 450 ± 7 | [3] | 12°30′25″ | 42°09′04″ | 0.71092 | 0.51210 |
| SPX37 | Fall F Unit | Fall F | 447 ± 7 | [3] | 12°30′00″ | 42°00′33″ | 0.71113 | 0.51211 |
| SPX39 | Sant'Abbondio $_{base}$ | SAAS $_{base}$ | 389 ± 4 | [3] | 12°29′31″ | 42°13′11″ | 0.71128 | |
| SPX41 | Sant'Abbondio $_{top}$ | SAAS $_{top}$ | 379 ± 40 | [3] | 12°29′31″ | 42°13′11″ | 0.71052 | 0.51211 |
| SPX43 | Cornazzano lava | | 329 ± 4 | [7] | 12°16′20″ | 42°′01′06″ | 0.71040 | 0.51210 |
| SPX49 | Tufo di Bracciano Unit | | 325±2 | [8] | 12°10′12″ | 42°02′51″ | 0.71090 | |
| SPX44 | Monte Musino scoria cone | | 318±6 | [7] | 12°26′17″ | 42°06′08″ | 0.71072 | 0.51209 |
| SPX45 | Monte Rocca Romana Lava | | 317 ± 14 | [7] | 12°14′48″ | 42°10′23″ | 0.70959 | 0.51213 |
| SPX47 | Magliano Romano Plinian fall | MRP | 312 ± 2 | [7] | 12°25′22″ | 42°08′34″ | 0.71040 | 0.51210 |
| SPX51 | Monte Aguzzo Scoria cone | | 302 ± 6 | [7] | 12°24′58″ | 42°03′47″ | 0.71049 | |
| SPX53 | Aguscello maar succession | | 298 ± 3 | [7] | 12°14′19″ | 42°12′30″ | 0.71101 | 0.51211 |
| SPX55 | Tufo Giallo di Sacrofano | TGDS | 287 ± 2 | [7] | 12°25′22″ | 42°08′34″ | 0.71064 | 0.51210 |
| SPX54 | Vigna di Valle Lava | | 285 ± 6 | [7] | 12°15′54″ | 42°05′26″ | 0.71062 | 0.51210 |
| SPX57 | Tufo di Pizzo Prato | | 251 ± 16 | [7] | 12°16′35″ | 42°05′25″ | 0.71122 | 0.51211 |
| SPX59 | Monte Maggiore scoria cone | | 207 ± 7 | [7] | 12°25′28″ | 42°08′25″ | 0.71009 | 0.51210 |
| SPX61 | Tufo di Vigna di Valle | | 194 ± 7 | [7] | 12°15′52″ | 42°05′21″ | 0.71061 | |
| SPX63 | Lagusiello maar succession | | 159 ± 4 | [7] | 12°17′16″ | 42°09′14″ | 0.71109 | 0.51210 |
| SPX62 | Cornacchia Lava | | *154 ± 7* | [9] | 12°13′10″ | 42°13′00″ | 0.71063 | 0.51210 |
| SPX64 | Prato Fontana Lava | | *134 ± 33* | [9] | 12°18′54″ | 42°11′53″ | 0.71058 | 0.51210 |
| SPX65 | Baccano Lower Unit | | 132 ± 2 | [7] | 12°22′03″ | 42°05′42″ | 0.70954 | 0.51214 |
| SPX71 (cpx d) | Baccano Main Unit | | 99 ± 3 | [10] | 12°22′36″ | 42°07′34″ | 0.71030 | 0.51211 |
| SPX71 (cpx l) | Baccano Main Unit | | 99 ± 3 | [10] | 12°22′36″ | 42°07′34″ | 0.71064 | 0.51210 |
| SPX67 | Stracciacappa Maar Unit | | 98 ± 4 | [7] | 12°19′03″ | 42°08′07″ | 0.71033 | 0.51212 |
| SPX69 | Monte Broccoleto scoria cone | | 94 ± 5 | [7] | 12°26′17″ | 42°06′08″ | 0.71060 | 0.51210 |
| SPX73 | Martignano Upper Unit | | 70 ± 3 | [10] | 12°18′34″ | 42°06′12″ | 0.71025 | 0.51212 |

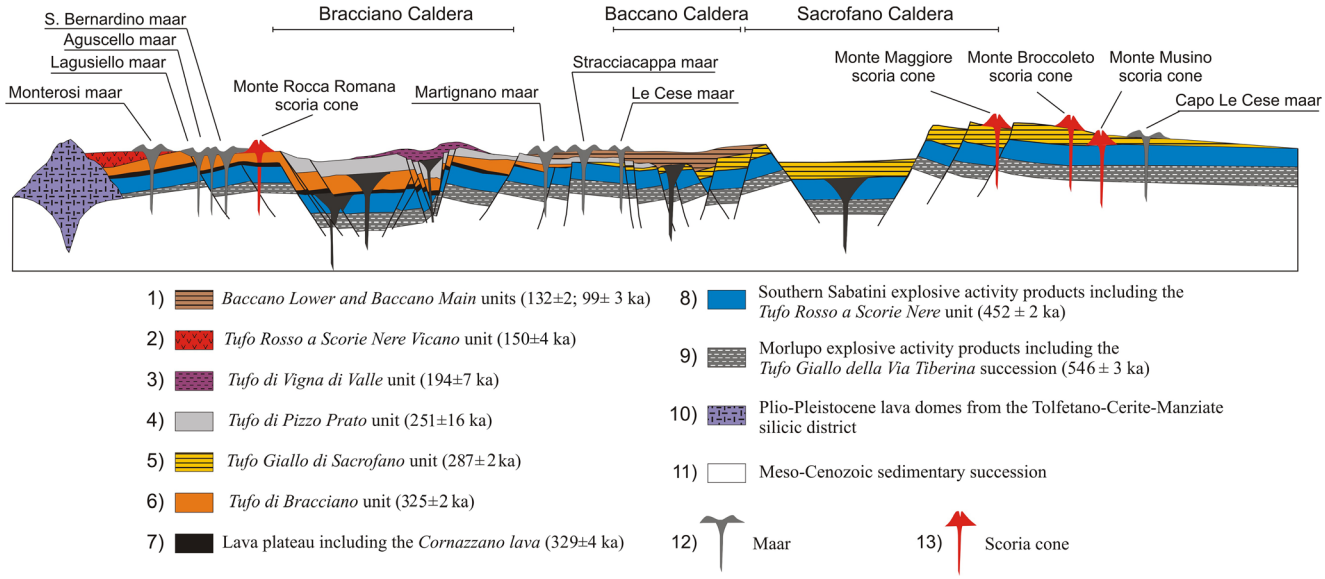


**Fig. 2** Key stratigraphic relationships among the main products from the SVD activity periods along a broadly W–E-oriented section across the whole district (modified after *Sottili* et al., (2010a); fully referenced geochronological data are reported in Table 1)

– The Grottarossa Pyroclastic Sequence (510 ± 4 ka) consists of repeated alternances of centimeter- to decimeter-thick dark gray ash layers and scoria lapilli fallout beds, imparting a well-stratified appearance (Marra et al. 2014)

## Southern Sabatini activity (~ 500 to ~ 400 ka)

This highly explosive period, sourced in the central-southern sector of the SVD (Fig. 1), marked the SVD climax of activity in terms of eruption intensities and magnitudes (Sottili et al. 2004). It was characterized by the emplacement of widespread sub-Plinian and Plinian fall deposits (VEI 3-5), with recurrence intervals of the order of $10^4$ years and W-E-trending dispersal axes (Sottili et al. 2004). The main SVD caldera-forming explosive event also took place during this period. Recent papers record widespread tephra occurrences in the Mediterranean area related to the Southern Sabatini activity period (Giaccio et al. 2014; Petrosino et al. 2014; Leicher et al. 2015). The stratigraphic succession includes six fall units from major explosive events (A through F) and one eruptive unit associated with the most important caldera-forming event. This is, from base to top:

– Fall A (498 ± 2) overlies a mature dark-brown paleosoil developed on top of the Grottarossa Pyroclastic Sequence (see above) and consists of two fallout subunits (A1 and A2; Sottili et al. 2004), both made up of multiple beds with changes in pumice color from whitish to gray upward (Di Rita and Sottili 2019; Marra et al. 2014). The A1 deposits, with an estimated volume of ~ 1.9 $km^3$ DRE (Sottili et al. 2004), have been also recognized in tephra records from the Acerno and Mercure basins, southern Italy (Giaccio et al. 2014; Petrosino et al. 2014), and in the Balkan Peninsula (lake Ohrid, Leicher et al. 2015)
– Fall B (494 ± 14), separated by the underlying Fall A by a mature paleosoil, consists of four subunits (B1 to B4; Sottili et al. 2004), each made up of a discrete decimeter-thick pumice fall bed, phonolitic in composition (Marra et al. 2014). The total volume, as determined from isopach maps, is in the order of 4 $km^3$ DRE (Sottili et al. 2004)
– Fall C (461 ± 2, Marra et al. 2017), separated from Fall B by an intervening mature paleosoil, consists of two subunits (C1 and C2; Sottili et al. 2004), showing a stratified texture imparted by multiple clast grading and compositional zoning (from whitish pumice to dark scoria lapilli upward) and a total thickness of ~ 2 m
– The Tufo Rosso a Scorie Nere eruptive unit (452 ± 2 ka) is derived from the most important caldera-forming event in the SVD (Palladino et al. 2014) and comprises two main flow units: the lower one, typically welded with gray fiamme is also known as Peperini Listati (Cioni et al. 1993; de Rita et al. 1993) and is exposed locally in the eastern SVD sector. The upper one is by far the most widespread, is known as Tufo Rosso a Scorie Nere, and is characterized by black scoria blocks embedded in a reddish matrix lithified due to vapor phase zeolite crystallization (Sottili et al. 2004). The Tufo Rosso a Scorie Nere rests on top of co-eruptive Fall D (Sottili et al. 2004), emplaced during the mostintense SVD Plinian event, with a column height reaching up to 29 km and VEI 4–5 (Sottili et al. 2004; Marra et al. 2014)
– Fall E (450 ± 7 ka) occurs in the eastern SVD sector, bounded by an erosional surface from the underlying Tufo Rosso a Scorie Nere. It consists of a single, up to

60-cm-thick, whitish pumice fallout unit, phonolitic in composition (Marra et al. 2014)
- Fall F (447 ± 7 ka), exposed in the southern and eastern SVD, consists of a ~ 50-cm-thick pumice fall deposit, with intervening thin (< 1 cm-thick) ash layers (Marra et al. 2014)

The post-climactic Southern Sabatini explosive activity (389 ± 4–379 ± 40 ka) is represented by a ~ 10-m-thick pyroclastic succession, informally named Sant'Abbondio Ash-Lapilli Succession (Marra et al. 2014), which overlies two Plinian fall deposits from the Vico Volcanic District (i.e., the 419 ± 6 ka Vico α and the 403 ± 6 ka Vico β; Cioni et al. 1993; Barberi et al. 1994; Marra et al. 2014), and it is topped by the 312 ± 2 ka Magliano Romano Plinian fall deposit (Sottili et al. 2010a).

## Sacrofano caldera activity (~ 300 to ~ 200 ka)

The Sacrofano Caldera developed between 300 and 200 ka in the eastern-central sector of the SVD (Figs. 1 and 2). This period of activity was mostly characterized by dominant Strombolian and hydromagmatic activity and subordinate Plinian and sub-Plinian events (Marra et al. 2014). The following units have been recognized in stratigraphic order:

- Monte Musino scoria cone (318 ± 6 ka), located along the south-eastern rim of the Sacrofano caldera, and associated to a small lava flow underlying the Tufo Giallo di Sacrofano (related to a major caldera-forming eruption, Sottili et al. 2010a)
- Magliano Romano Plinian fall (312 ± 2 ka), cropping out extensively in the north-eastern sector of the SVD, often underlying the Tufo Giallo di Sacrofano, an important marker horizon for the post-Southern Sabatini stratigraphy (i.e., younger than ~ 400 ka; Sottili et al. 2010a). Along the northern rim of the Sacrofano caldera, it reaches a maximum thickness of ~ 2 m (Sottili et al. 2010a)
- Monte Aguzzo Scoria cone (302 ± 6 ka), located ~ 4 km from the southern rim of the Sacrofano caldera (Sottili et al. 2010a)
- The Tufo Giallo di Sacrofano (287 ± 2 ka) was emplaced during a major caldera-forming event at 287 ± 2 ka (Sottili et al. 2010a) and partly buried older eruptive centers and crater morphologies. It covers an area of some hundred square kilometers around the present caldera (Sottili et al. 2010a), including the north-eastern part of the Rome urban area (Karner et al. 2001)
- The well-preserved Monte Maggiore scoria cone (208 ± 7 ka) was produced by Strombolian and effusive activities along the northern caldera rim (Sottili et al. 2010a) following the Tufo Giallo di Sacrofano (Fig. 2)

## Bracciano caldera activity (~ 325 to ~ 200 ka)

This period of activity, nearly contemporaneous to the Sacrofano caldera activity, is associated with the formation of the main SVD caldera (approximately ~ 10 km in diameter), which presently hosts the Bracciano Lake (Fig. 1; de Rita et al. 1993, 1996). The Bracciano Caldera activity ended with dominantly Strombolian/effusive and subordinately hydromagmatic eruptions from either scattered or clustered monogenetic centers aligned along the ring fault systems bordering the area North of Bracciano lake (Sottili et al. 2012). The following units and associated morphologies have been distinguished:

- The Cornazzano lava (329 ± 4 ka), which is part of a lava plateau covering an area > 120 $km^2$ South-West of Bracciano Lake (Sottili et al. 2010a)
- The Monte Rocca Romana scoria cone (609 m a.s.l.) is located just to the North of Bracciano Lake. A lava flow that crops out on the south-eastern slope of the scoria cone, with an estimated volume of ~ 0.12 $km^3$ DRE, has been dated at 317 ± 14 ka (Sottili et al. 2010a).
- The Tufo di Bracciano (325 ± 2 ka, Pereira et al. 2017) was emplaced during the main caldera-forming event of this period (Sottili et al. 2010a). The main pyroclastic flow unit crops out extensively at the top of the SVD volcanic succession to the North and West of Lake Bracciano, as far as the Tyrrhenian coastal plain (Fig. 1)
- The Aguscello maar (298 ± 3 ka) formed ~ 3 km North of Bracciano lake. The present-day crater, approximately 1 km in diameter, is rimmed by a stratified pyroclastic succession, > 10 m thick, made up of alternating centimeter-to decimeter-thick planar- to cross-laminated ash layers and decimeter-thick massive, clast-supported scoria lapilli beds, rich in accessory lithics with occasional impact sags (Sottili et al. 2012)
- The Vigna di Valle lava (285 ± 6 ka) crops out along the southwestern and southern shores of Bracciano lake, with a maximum exposed thickness of ~ 10 m (Sottili et al. 2010a)
- The Tufo di Pizzo Prato (251 ± 16 ka) is associated to a late caldera-forming event in the southeastern sector of the Bracciano caldera (Sottili et al. 2010a)
- The Tufo di Vigna di Valle (194 ± 7 ka) occurs on top of the Tufo di Pizzo Prato, along the external rims of a semicircular volcanic depression in the southern portion of the Bracciano caldera

## Late activity (~ 150 to ~ 70 ka)

The most recent SVD activity was characterized by low-magnitude eruptions from several, scattered or clustered,

monogenetic centers around the Bracciano and Sacrofano calderas (Fig. 2). Its lower age boundary is defined by the radiometric age of the Tufo Rosso a Scorie Nere Vicano (150 ± 4 ka; Laurenzi and Villa 1987) from the nearby Vico Volcanic District (Fig. 1), which represents a fundamental marker horizon for the reconstruction of the late SVD activity (Nappi and Mattioli 2003; Sottili et al. 2012). Hydromagmatic, Strombolian, and associated effusive eruptions formed well-preserved cinder cones, tuff rings, and subordinate tuff cones, scattered over an area of approximately 150 $km^2$:

– The Cornacchia lava (154 ± 7 ka), exposed ~ 7 km north-east of Bracciano lake northern shore directly on top of the Tufo Rosso a Scorie Nere Vicano with a maximum thickness of ~ 5 m (Nappi and Mattioli 2003). The Lagusiello Maar (159 ± 4 ka), characterized by hydromagmatic products cropping out around a horseshoe-shaped crater wall, with a maximum thickness of ~ 30 m, on top of a dark-brown mature paleosoil (Sottili et al. 2010a). The Prato Fontana lava (134 ± 33 ka) crops out in the northern SVD area, near the Monterosi Lake, overlying the Tufo Rosso a Scorie Nere Vicano, with a maximum thickness of ~ 5 m (Nappi and Mattioli 2003). The Baccano Lower and Baccano Main units (respectively, 132 ± 2 and 99 ± 3 ka, Marra et al. 2019), represent a complex pyroclastic succession marked by multiple erosional unconformities and paleosoils (including a dark-brown paleosoil between the Lower and Main units), related to a composite maar-caldera system (de Rita et al. 1993; Sottili et al. 2010a; Buttinelli et al. 2011; Palladino et al. 2015). The Stracciacappa Maar (98 ± 4 ka) is the youngest polygenetic maar in the central SVD area (Valentine et al. 2015). Its well-preserved flat-floored crater hosted a lake until it was drained in AD 1834 (Sottili et al. 2010a). The Monte Broccoleto scoria cone (94 ± 5 ka), located south-east of the Sacrofano caldera, comprises poorly consolidated Strombolian fallout deposits and a small lava flow (Sottili et al. 2010a). The Martignano maar, located to the East of Bracciano Lake, shows composite volcanic morphologies with at least three coalescing craters, overall 2.5 km across (Sottili et al. 2010a). The Martignano Upper Unit (70 ± 3 ka; Marra et al. 2019) represents the youngest eruptive event dated up to now in the SVD.

## Sample selection

In order to perform chemical and isotopic analyses on volcanic products representative of the whole SVD activity, clinopyroxene crystals (a ubiquitous mineral phase in the whole liquid line of descent of potassic magmatism) have been selected from rock samples of the units with available geochronological age. In Table 1, outcrop locations, $^{40}Ar/^{39}Ar$ ages, and isotopic data are reported for all the sampled products. Table 1 reports the main depositional features of the sampled materials along with the ascription of the samples to individual eruptive units within the framework of the SVD activity periods.

Four samples have been selected from the SVD Paleo-activity. SPX 1 is a primary or partially reworked pumice fall deposit, on top of the upmost gravel layer of the Paleo-Tiber 2 unit. Consistent with its age of 808 ± 6 ka on sanidine (Karner et al. 2001), it is the stratigraphically lowest among the dated tephra layers. SPX 3 is a primary, 20-cm-thick, ash matrix-supported pyroclastic layer yielding age of 800 ± 11 ka on sanidine (Karner et al. 2001); SPX 5 was collected from a 20–30-cm-thick, partially reworked volcaniclastic layer intercalated in the basal gravel layer of the Paleo-Tiber 3 aggradational succession (PG2 Formation) in the Ponte Galeria area, with a weighted mean age of 763 ± 8 ka (Karner et al. 2001); SPX 7, dated at 653 ± 4 ka (Karner et al. 2001), was collected from a ~ 1-m-thick pyroclastic flow deposit recovered in borehole in southern Rome, intercalated within the Paleo-Tiber 4 aggradational succession (Santa Cecilia Formation, Karner and Marra 1998).

A total of 36 other samples were selected from the Morlupo, Southern Sabatini, Sacrofano Caldera Bracciano Caldera, and SVD Late activities, as listed in Table 1.

## Analytical methods

Chemical analyses of clinopyroxene crystals were performed at the Consiglio Nazionale delle Ricerche—Istituto di Geologia Ambientale e Geoingegneria (CNR-IGAG) c/o Dipartimento di Scienze della Terra, Sapienza-University of Rome, Italy) with a Cameca SX50 electron microprobe equipped with five wavelength-dispersive spectrometers using 15 kV accelerating voltage, 15 nA beam current, 10 μm beam diameter, and 20-s counting time. The following standards were used: wollastonite (Si and Ca), corundum (Al), diopside (Mg), andradite (Fe), rutile (Ti), orthoclase (K), jadeite (Na), barite (Ba), celestine (Sr), F-phlogopite (F), baritine (S), and metals (Cr and Mn). Ti and Ba contents were corrected for the overlap of the TiKα and BaKα peaks.

Sr and Nd isotopic compositions were determined by thermal ionization mass spectrometry. Mineral fractions of 0.1 g were ultrasonically cleaned in diluted hydrofluoric acid (7%) and then rinsed with MilliQ® water, before chemical dissolution with a mixture of ultrapure acids ($HF$-$HNO_3$-$HCl$). Chemical dissolution and Sr and Nd separation by conventional ion-exchange chromatographic techniques were performed in the laboratories of the Istituto Nazionale di Geofisica e Vulcanologia, Osservatorio Vesuviano (INGV, OV). $^{87}Sr/^{86}Sr$ isotope ratios were measured by using a

Finnigan MAT 262 multicollector mass spectrometer at CNR-IGAG (c/o Dipartimento di Scienze della Terra, Sapienza-University of Rome) and at the Consiglio Nazionale delle Ricerche—Istituto di Geoscienze e Georisorse (IGG–CNR; Pisa). $^{143}Nd/^{144}Nd$ values were measured at the Istituto Nazionale di Geofisica e Vulcanologia, Osservatorio Vesuviano (INGV, OV). The measured Sr isotope ratios are considered to be free of inter-laboratory bias since during the collection of isotopic data, replicate analyses of NIST-SRM 987 ($SrCO_3$) have been performed at both laboratories to check for external reproducibility. The $2\sigma_{mean}$, i.e., the standard error relative to Sr and Nd isotope ratio determinations, with N = 180, is better than ± 0.000010 for Sr and ± 0.000006 for Nd measurements. Moreover, the mean measured values of $^{87}Sr/^{86}Sr$ for NIST-SRM 987 and of $^{143}Nd/^{144}Nd$ for La Jolla, during the period of measurements, were 0.710215 ± 0.000017 (2σ, N = 18), 0.710200 ± 0.000012 (2σ, N = 22), and 0.511845 ± 0.000010 (2σ, N = 42), respectively. Measured $^{87}Sr/^{86}Sr$ and $^{143}Nd/^{144}Nd$ isotope ratios were normalized for within-run isotopic fractionation to $^{86}Sr/^{88}Sr$ = 0.1194 and $^{146}Nd/^{144}Nd$ = 0.7219, respectively. The external reproducibility 2σ (i.e., maximum ± 0.000017 for Sr and ± 0.00001 for Nd) was calculated according to Goldstein et al. (2003) and represents the measurements errors. These errors are reported in Fig. 6 as error bars. However, in the case of Sr measurements, the error bars are within the symbols. Sr and Nd isotope ratios have been normalized to the recommended values of NIST-SRM 987 ($^{87}Sr/^{86}Sr$ = 0.71025) and La Jolla ($^{143}Nd/^{144}Nd$ = 0.51185) standards, respectively (Thirlwall 1991). Total procedural blanks were below 2 ng Sr and 1 ng Nd for all the samples. Results are reported in Table 1.

## Results

In the following two sections, we report the results from geochemical analyses of clinopyroxene, including $^{87}Sr/^{86}Sr$ and $^{143}Nd/^{144}Nd$ isotope compositions, within the context of the six main phases of activity of the SVD.

### Geochemistry of clinopyroxene

The representative compositions and the complete dataset of the SVD clinopyroxene and glass compositions are reported in Table 2, while in Figs. 3 and 4, their main chemical features are plotted. Figure 1A (Electronic Supplementary Material 3) a reports the total alkali-silica classification diagram (TAS; Le Bas et al. 1986) showing the composition of matrix glasses of the Sabatini juveniles. In the conventional Wo-En-Fs diagram (quadrilateral, Q, components of Morimoto 1988), the SVD clinopyroxenes fall into the diopside field (Fig. 3), even if they are characterized by high contents of extra Q components (e.g., esseneite up to 32 mol%, Ca-Tschermak up to 15 mol%). The M1 site is mainly occupied by Mg (0.468–0.976 apfu) with relatively minor amounts of $Fe^{2+}$ (0.000–0.290) and $R^{3+}$ (0.018–0.428), where $R^{3+}$ is $Cr^{3+} + Al^{3+} + Ti^{4+} + Fe^{3+}$. The M2 site is occupied by Ca (0.908–0.992 a.f.u.) and minor amounts of Na (0.004–0.042 apfu). The tetrahedral site is characterized by relatively low Si contents (1.607–1.971 apfu: atoms per formula unit) and is occupied by 2.00 by aluminum. For the most part, the analyzed clinopyroxenes crystallized in equilibrium with differentiated magmas at low pressure, as indicated by the increase of Na and Al contents with decreasing Mg# (Mg/(Mg + $Fe_{tot}$) value and by the low ratio $Al^{VI}/Al^{IV}$ (Fig. 4). Also, Fe–Mg ratio of glasses and clinopyroxenes in the Sabatini juveniles (see table in Appendix). Also, the value of $^{cpx–melt}Kd_{Fe–Mg}$ (~ 0.22) closely match the equilibrium range 0.28 ± 0.08 of the Fe–Mg exchange reaction [$^{cpx–melt}Kd_{Fe–Mg} = (Fe_{cpx}\ Fe_{melt}) \times (Mg_{melt}\ Mg_{cpx})$] (Fig. 2a). However, the occurrence of Cr-rich clinopyroxene in the youngest hydromagmatic products, as well as in the Tufo Giallo della Via Tiberina granular enclaves, indicates that batches of primitive magmas have refilled periodically the SVD plumbing system. The latter is certainly a dynamic and open differentiation magmatic system as indicated by the occurrence of different clinopyroxene populations in some eruptive units. In Fall F, for example, textural features and backscattered images (Fig. 5) discriminate three distinct clinopyroxene populations. Type 1 appear as euhedral, coarse (> 1 mm in size) clinopyroxenes with a direct (i.e., decrease of Mg# toward the rim) oscillatory zoning (Fig. 5a). Type 2 occurs as millimeter-sized crystals with a weak reverse zoning and, occasionally, with spongy cellular textures associated with patchy zoning, possibly in response to disequilibrium events (Fig. 5b). Type 3 are homogeneous, Mg#-rich crystals with spongy cellular core surrounded by euhedral rim (Fig. 5c). In contrast, other eruptive units (e.g., Fall E and Tufo Rosso a Scorie Nere) show relatively homogeneous clinopyroxenes (Fig. 5d).

### Isotopic evolution of the Sabatini Volcanic District

The measured $^{87}Sr/^{86}Sr$ ratio in clinopyroxene from SVD volcanics, spanning in age between 808 ± 6 ka and 70 ± 3 ka, ranges between 0.7115 and 0.7095 (Fig. 6; Table 1). This is very close to that obtained by considering all previous works on bulk lava samples from the SVD (i.e., 0.7112–0.7092; Hawkesworth and Vollmer 1979; Conticelli et al. 1997, 2002, 2015; Del Bello et al. 2014). Samples from the Paleo-activity are characterized by high $^{87}Sr/^{86}Sr$ (from 0.71128 to 0.71140) and a constant, within analytical errors, $^{143}Nd/^{144}Nd$ ratio (~ 0.51213). The early subphase (~ 590 ka) of the Morlupo Activity erupted magmas isotopically similar, in terms of both Sr and Nd, to those of the Paleo-activity. During the middle subphase (~ 550 ka), including the Lower Tufo Giallo Della Via Tiberina and the Sella di Corno Plinian

**Table 2** Representative EMP analyses of SVD clinopyroxenes[a]

| | TGCP | | TGPP | | Fall C | Fall D | Tufo di Pizzo prato | | Tufo di Bracciano Unit | |
|---|---|---|---|---|---|---|---|---|---|---|
| | Core | Core | Core | Core | Core | Core | Core | Rim | Core | Rim |
| $SiO_2$ | 44.24 | 46.83 | 50.50 | 49.38 | 41.56 | 48.20 | 45.26 | 44.52 | 51.38 | 46.91 |
| $TiO_2$ | 1.34 | 0.95 | 0.53 | 0.78 | 2.03 | 0.80 | 1.48 | 1.61 | 0.47 | 1.15 |
| $A_{l2}O_3$ | 9.06 | 6.57 | 3.66 | 5.44 | 9.41 | 4.80 | 6.80 | 7.49 | 3.46 | 6.87 |
| FeO | 10.41 | 8.73 | 5.80 | 6.51 | 15.66 | 8.87 | 12.77 | 13.79 | 4.76 | 9.25 |
| MnO | 0.24 | 0.13 | 0.13 | 0.07 | 0.52 | 0.22 | 0.70 | 0.73 | 0.05 | 0.21 |
| MgO | 10.53 | 12.50 | 15.20 | 13.99 | 6.74 | 13.03 | 9.20 | 8.77 | 15.59 | 11.77 |
| CaO | 23.59 | 23.37 | 24.39 | 24.29 | 23.38 | 24.48 | 22.80 | 22.84 | 23.95 | 23.92 |
| $Na_2O$ | 0.23 | 0.22 | 0.12 | 0.18 | 0.50 | 0.18 | 0.54 | 0.54 | 0.12 | 0.24 |
| $K_2O$ | 0.00 | 0.01 | 0.01 | 0.02 | 0.00 | 0.00 | 0.03 | 0.00 | 0.00 | 0.01 |
| $Cr_2O_3$ | 0.00 | 0.00 | 0.00 | 0.00 | 0.00 | 0.00 | 0.02 | 0.00 | 0.47 | 0.00 |
| | 99.63 | 99.30 | 100.34 | 100.66 | 99.80 | 100.58 | 99.59 | 100.29 | 100.24 | 100.33 |
| 6-oxygen formula | | | | | | | | | | |
| Si | 1.666 | 1.754 | 1.849 | 1.810 | 1.602 | 1.791 | 1.726 | 1.691 | 1.880 | 1.747 |
| Ti | 0.038 | 0.027 | 0.015 | 0.022 | 0.059 | 0.022 | 0.042 | 0.046 | 0.013 | 0.032 |
| Al IV | 0.334 | 0.246 | 0.151 | 0.190 | 0.398 | 0.216 | 0.274 | 0.309 | 0.120 | 0.253 |
| Al VI | 0.068 | 0.044 | 0.007 | 0.045 | 0.029 | .000 | 0.032 | 0.026 | 0.029 | 0.048 |
| $Fe^{3+}$ | 0.207 | 0.166 | 0.123 | 0.116 | 0.289 | 0.191 | 0.199 | 0.231 | 0.061 | 0.159 |
| $Fe^{2+}$ | 0.120 | 0.108 | 0.054 | 0.084 | 0.215 | 0.083 | 0.208 | 0.208 | 0.085 | 0.129 |
| Mn | 0.007 | 0.004 | 0.004 | 0.002 | 0.017 | 0.007 | 0.023 | 0.023 | 0.001 | 0.007 |
| Mg | 0.591 | 0.698 | 0.830 | 0.764 | 0.387 | 0.719 | 0.523 | 0.497 | 0.851 | 0.653 |
| Ca | 0.952 | 0.938 | 0.957 | 0.954 | 0.965 | 0.971 | 0.932 | 0.929 | 0.939 | 0.954 |
| Na | 0.016 | 0.016 | 0.009 | 0.013 | 0.038 | 0.013 | 0.040 | 0.040 | 0.009 | 0.017 |
| K | 0.000 | 0.000 | 0.001 | 0.001 | 0.000 | 0.000 | 0.001 | 0.000 | 0.000 | 0.001 |
| Cr | 0.000 | 0.000 | 0.000 | 0.000 | 0.000 | 0.000 | 0.001 | 0.000 | 0.014 | 0.000 |
| | 4.000 | 4.000 | 4.000 | 4.000 | 4.000 | 4.000 | 4.000 | 4.000 | 4.000 | 4.000 |

*TGCP* Tufo Giallo di Castelnuovo di Porto unit, *TGPP* Tufo Giallo di Prima Porta unit

[a] EMP analyses of clinopyroxenes occurring in the SVD eruptive units and do not shown in the table, are reported in Masotta et al. (2010); Sottili et al. (2012); Palladino et al. (2014)

Fall, magmas less enriched in radiogenic Sr (~0.71030) and unradiogenic Nd (~0.51210) were erupted. The late Morlupo subphase (~510 ka) was characterized by magmas with Sr isotope ratios ranging from 0.71120 to 0.71080 and Nd isotope ratios of ~0.51210. The early Southern Sabatini activity (i.e., including Fall A and B), similarly to the preceding period, started with eruptive products characterized by $^{87}Sr/^{86}Sr$ of ~0.7114 and relatively low $^{143}Nd/^{144}Nd$, similar

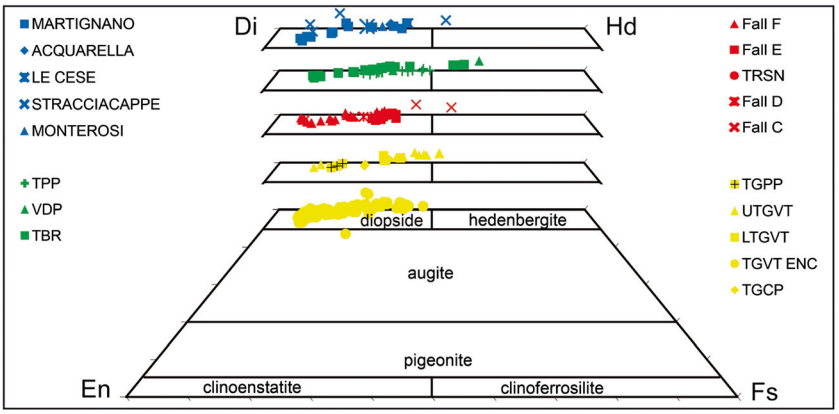


**Fig. 3** Diopside (Di)-Hedembergite (Hd)-Enstatite (En)-ferrosilite (Fs) classification diagram (Morimoto 1988) of clinopyroxenes from SVD rock types

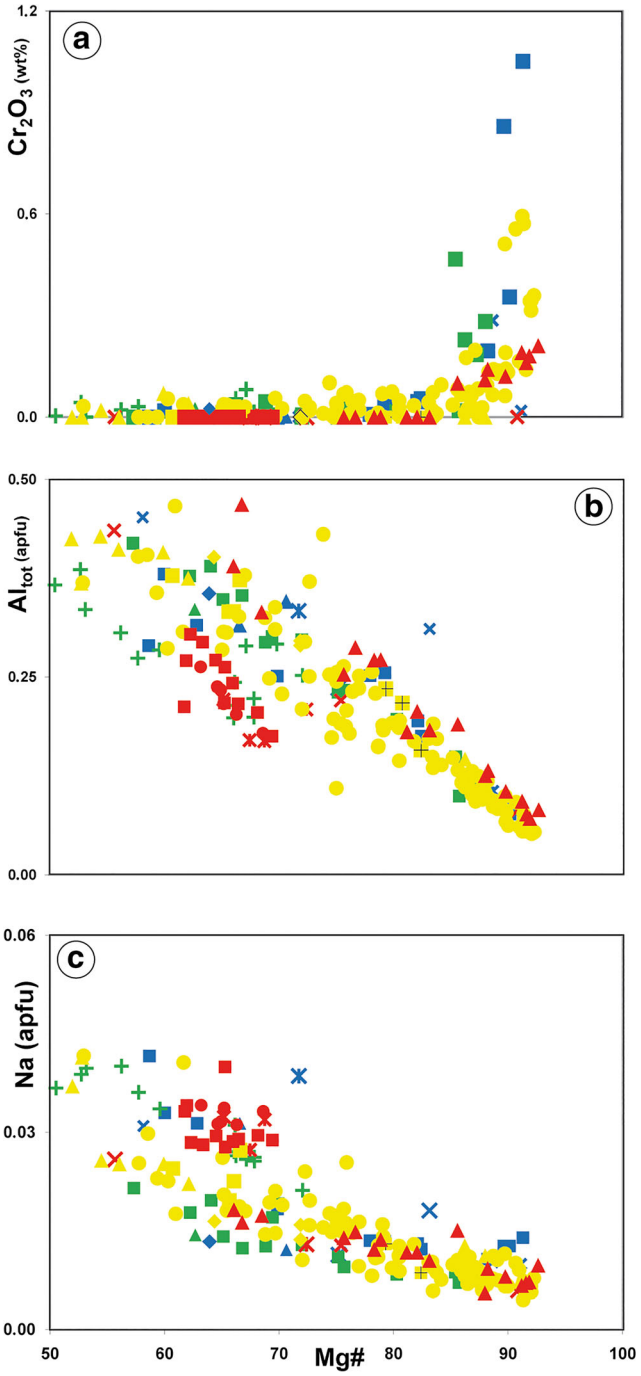


**Fig. 4** Binary covariation plots of Mg# vs. $Cr_2O_3$ (**a**), $Al_{tot}$ (**b**), and Na (**c**) for clinopyroxene crystals sampled from SVD eruptive products. Mg# is calculated as Mg/(Mg + $Fe_{tot}$) * 100. The arrow in **b** indicates the onset of plagioclase crystallization in equilibrium with clinopyroxene in the SVD magmas

to the preceding late subphase of the Morlupo activity (Fig. 6; Table 1). During the following Southern Sabatini eruptions (i.e., from Fall C to Fall F), the Sr isotope ratio increased from 0.7104 to 0.7111, at relatively constant Nd isotope ratios (Table 1). Notably, the Sant'Abbondio Ash-lapilli Succession was characterized by high $^{87}Sr/^{86}Sr$ (~0.71130) and constant Nd (~0.51210) at the base (SPX 39, 389 ± 4 ka), and a significantly lower $^{87}Sr/^{86}Sr$ (~0.71052) at top with respect to the climactic Southern Sabatini activity.

The onset of activity from Sacrofano and Bracciano calderas (nearly contemporaneous in the time span of ~350–190 ka) was characterized by $^{87}Sr/^{86}Sr$ similar to those of the San Abbondio Ash-lapilli Succession top deposit (i.e., ~0.71070 for the Monte Musino scoria cone of the Sacrofano Caldera activity and ~0.71040 for the Cornazzano lava of the Bracciano caldera activity). During the Sacrofano Caldera activity, the eruptive products show isotopic ratios varying from ~0.7107 to ~0.7101, which irregularly decreased until the youngest Monte Maggiore Scoria cone ($^{87}Sr/^{86}Sr$ ~ 0.71008). Instead, during the Bracciano Caldera activity, the $^{87}Sr/^{86}Sr$ isotope ratios range 0.71120–0.70960 there being no simple decreasing temporal trend between 350 and 190 ka (Fig. 6; Table 1). During the Bracciano and Sacrofano activities, Nd isotope ratios display no significant variations, with the exception of the least enriched in radiogenic Sr, the Monte Rocca Romana lava sample, which has the highest $^{143}Nd/^{144}Nd$ ratio (0.5121) and the lowest $^{87}Sr/^{86}Sr$ ratio (0.7096).

Volcanic products of the Late activity were characterized by $^{87}Sr/^{86}Sr$ ranging from 0.7111 to 0.70950 and $^{143}Nd/^{144}Nd$ of ~0.5121. Although the analyzed samples display an inverse correlation between Sr and Nd isotopes, neither a linear time-dependent variation nor a relationship between Sr and Nd isotopes and source vent locations is observed.

In summary, considering the overall $^{40}Ar/^{39}Ar$ chronology of the main SVD periods of activity, $^{87}Sr/^{86}Sr$ and $^{143}Nd/^{144}Nd$ isotope ratios show a non linear, time-dependent decrease from the oldest to the youngest eruptive periods (Fig. 6). This variation is characterized by an albeit irregular decrease from the oldest to the youngest products.

## Discussion

The Roman Comagmatic province is the most thoroughly investigated potassic province in the world. Several volcanological and petrologic studies have attempted to clarify the genesis of the erupted magmas (e.g., Conticelli et al. 2002, 2015; Peccerillo and Frezzotti 2015). However, the origin of the geochemical signature of these magmas and whether this signature is acquired by magmas during their path toward the surface, or is a primary characteristic of their source, is still an open question. By assuming a "closed" mantle source model, Gaeta et al. (2016) estimated the age of the metasomatic event of the Roman province mantle source, based on the time interval required to shift from the 0.704 isotopic value of the depleted mantle to the 0.715 isotopic value of the phlogopite-rich mantle. Gaeta et al. (2016) suggested that the main event accounting for the mantle metasomatism occurred at 300 Ma,

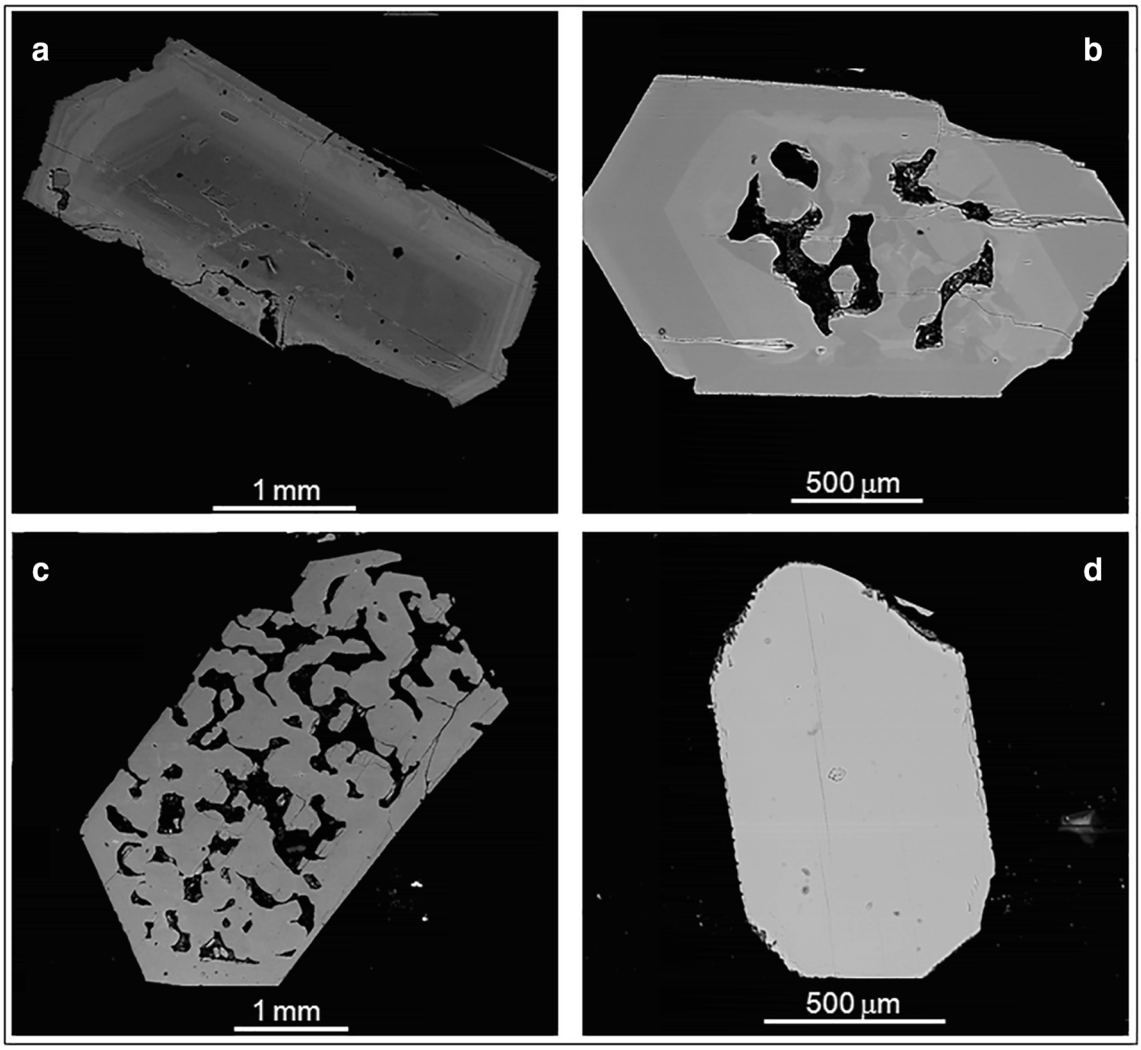


**Fig. 5** SEM backscattered SEM images of the clinopyroxenes occurring in Fall F (**a**–**c** photos) and in the Tufo Rosso a Scorie Nere (d photo). **a** Type 1 clinopyroxene with a direct (i.e., decrease of Mg# toward the rim) oscillatory zoning. **b** Type 2 clinopyroxene with a weak reverse zoning and spongy cellular texture. **c** Type 3 clinopyroxene with Mg#-rich composition and spongy cellular core surrounded by euhedral rim. **d** Homogenous clinopyroxene

whereas the subduction process, active during the Cenozoic-Quaternary age, was critical for triggering the Mediterranean ultrapotassic magmatism that shows both metasomatic and subduction-related geochemical signatures. The estimated age is similar to that suggested by Bell et al. (2013), who proposed a model in which fluids/melts enrichment is due to the late Triassic-early Jurassic Alpine Tethys plume activity beneath the Mediterranean basin. Furthermore, different ages for the metasomatic event, and/or models alternative to the subduction process, have been proposed in light of Nd and trace element trends at the Roman and Neapolitan volcanoes (e.g., Castorina et al. 2000; Avanzinelli et al. 2009; Mazzeo et al. 2014). In particular, the age of the enrichment event of the pre-subduction mantle source of the Neapolitan volcanoes has been calculated at 45 Ma (Mazzeo et al. 2014), thus justifying the poorly enriched signature of this mantle source with respect to that of the Roman province. Whatever the model, subduction related or not, the mantle metasomatism should be older than the onset of magmatic activity.

In the SVD, based solely on the effusive activity, Conticelli et al. (1997) distinguished a high-Ba and a low-Ba differentiation series, the former being also enriched in all the other incompatible elements, e.g., REE, Nb, Zr, Th except Rb. The high-Ba series comprises plagioclase-free, leucite-bearing lavas, whereas the low-Ba series includes plagioclase- and phlogopite-bearing lavas (Conticelli et al. 1997). The $^{87}Sr/^{86}Sr$ ratios in the high-Ba series lavas are higher (0.71047–0.71080) than in the Low-Ba series lavas (0.70944–0.71038) and do not vary significantly with magma differentiation. In previous works (Conticelli et al. 1997; Del Bello et al. 2014), no correlation was found between isotope compositions of the SVD-erupted products and their ages, while age-dependent isotope composition changes are well-known features of other Tuscan and Roman volcanoes, as

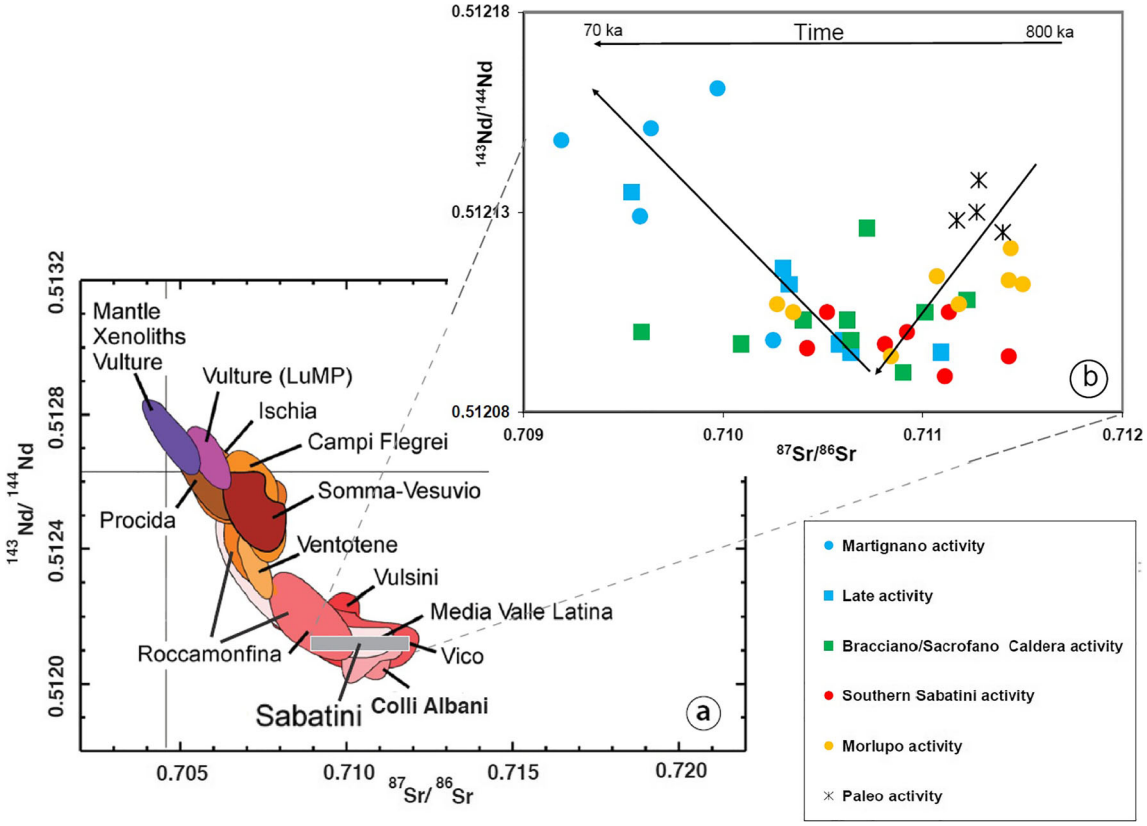


**Fig. 6** **a** $^{87}Sr/^{86}Sr$ vs. $^{143}Nd/^{144}Nd$ variations for the whole Roman and Campanian provinces, modified after Conticelli et al. (2010). **b** $^{87}Sr/^{86}Sr$ vs. $^{143}Nd/^{144}Nd$ of Sabatini magmas during the district history. Similarly to the Colli Albani volcanic district, the $^{87}Sr/^{86}Sr$ vs $^{143}Nd/^{144}Nd$ variation in the Sabatini is characterized by a change from a positive to a negative trend in the youngest magmas. Part of Martignano data are from Del Bello et al. (2014)

observed at Monte Amiata (Conticelli et al. 2015), Radicofani (Conticelli et al. 2010), Latera (Conticelli et al. 1991), Monte Cimino (Conticelli et al. 2010), Vico (Perini et al. 2004), Colli Albani (Gaeta et al. 2006, 2011, 2016; Boari et al. 2009), Middle Valle Latina (Boari et al. 2009), and Roccamonfina (Conticelli et al., 2009).

Here, we thus integrate the available isotope dataset on SVD lavas to provide a new comprehensive dataset for its pyroclastic units, thus obtaining a representative isotope characterization of the whole SVD, in the frame of the $^{40}Ar/^{39}Ar$ age setting (Table 1). This allows us to outline the time-dependent geochemical variations of the erupted magmas (Fig. 6) and discuss the analogy to the nearby Colli Albani Volcanic District (Gaeta et al. 2006, 2011, 2016).

## Source vs crustal isotopic fingerprinting

In Fig. 6, the relationship between Sr and Nd isotope ratios of SVD products, within the framework of Italian Queternary volcanism, is shown. Overall, both isotope ratios first decrease, as observed at Colli Albani, then $^{143}Nd/^{144}Nd$ increases while $^{87}Sr/^{86}Sr$ ratios continue to decrease. At Colli Albani, Gaeta et al. (2016) assumed the positive correlation between Nd and Sr isotopes as due to the presence of accessory phases, such as allanite, monazite, and apatite in the source rocks, which affected more efficiently the geochemical signal of early-erupted magmas. On the other hand, the negative $^{143}Nd/^{144}Nd$ - $^{87}Sr/^{86}Sr$ correlation observed in samples younger than 450 ka was attributed to the phlogopite and clinopyroxene (±olivine) control on the isotopic composition of the magmas. Similarly to the Colli Albani volcanics, SVD samples display an overall decrease in Sr isotopes when considering the mean $^{87}Sr/^{86}Sr$ of the pyroclastic products erupted during each period of activity (Fig. 7). Nevertheless, in the SVD, these variations are not simply correlated with time, and there is some scatter in the Sr data within each activity period (Fig. 6b).

The isotopic variations of the SVD erupted magmas are possibly due to the superposition of additional petrological processes with respect to those recognized at Colli Albani. In the latter district, evidence from cored bombs (i.e., scoria clasts hosting carbonate fragments with various degrees of decarbonation; Sottili et al. 2010b), occurrence of primary calcite in the lava flows, and many geochemical and experimental studies demonstrate an extensive interaction between magmas and carbonate crustal rocks (Dallai et al. 2004; Di

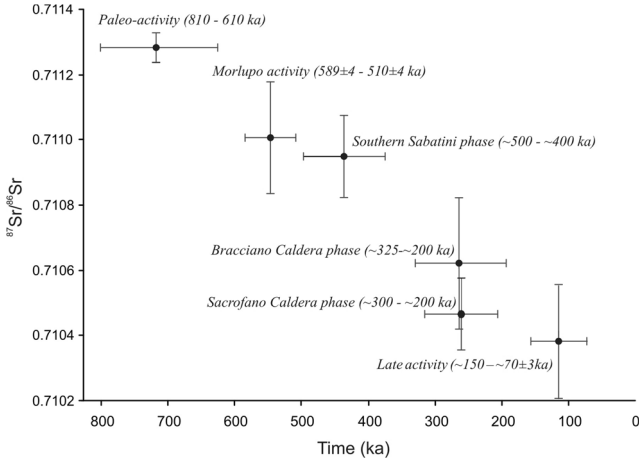


**Fig. 7** Time-dependent geochemical variations of $^{87}Sr/^{86}Sr$ ratio in clinopyroxene during the six main eruptive periods of the SVD. Vertical bars are the standard deviation of the mean (*SDM*) of the $^{87}Sr/^{86}Sr$ ratio (see Table 1); horizontal bars reflect the time duration of individual activity periods (the fully referenced radiometric age dataset is reported in Table 1)

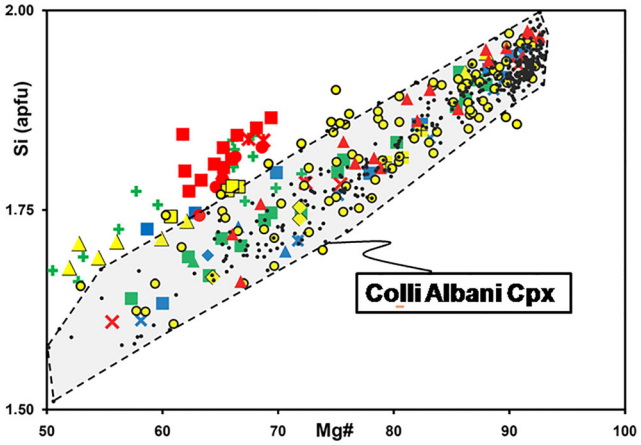


**Fig. 8** Binary covariation plot of Mg# vs. Si for clinopyroxene crystals from the SVD eruptive products. Mg# is calculated as Mg/(Mg + $Fe_{tot}$) * 100. The gray areas represent the chemical composition of Colli Albani clinopyroxenes (data from: Gaeta and Freda 2001; Gaeta et al. 2006, 2009; Di Rocco et al. 2012; Gozzi et al. 2014); apfu atoms per formula unit

Rocco et al. 2012; Cross et al. 2014; Freda et al. 1997; 2008; Gaeta et al. 2006, 2009; Gozzi et al. 2014; Iacono Marziano et al. 2007; Laurora et al. 2009; Mollo et al. 2010; Peccerillo and Frezzotti 2015).

Clinopyroxene chemistry indicates that SVD magmas have interacted with a crust of different composition. In general, the variations of Si vs. Mg# contents of the SVD clinopyroxene are similar to those in Colli Albani clinopyroxene. According to Gaeta et al. (2006), the positive correlation between Si (apfu) and Mg# mirrors the differentiation of the melt in equilibrium with clinopyroxene. In fact, phase equilibria experiments on a tephri-phonolitic scoria of the SVD (Masotta et al. 2010) indicate that the Mg# decrease parallels both the decreasing experimental temperature (i.e., from 1000 to 800 °C) and the changing composition from tephri-phonolite to phonolite of the melt in equilibrium with clinopyroxene.

In the natural SVD clinopyroxene, the evolutionary trend is clearly indicated by the correlation between Mg# and the $Cr_2O_3$ contents (Fig. 4). Nevertheless, SVD clinopyroxene, for a given Mg#, shows a wider Si range with respect to Colli Albani (Fig. 8), possibly indicating that magma differentiation in the SVD plumbing system was driven by the crystallization of different mineral phases with respect to Colli Albani. In particular, the high silica activity in the SVD magmas (Masotta et al. 2010; Palladino et al. 2014) forces the reaction $CaAl_2Si_2O_{8\ (An)} = CaAl_2SiO_{6\ (Cpx)} + SiO_{2\ (Liquid)}$ toward an early crystallization of plagioclase. The onset of plagioclase crystallization in the SVD magmas occurs when the crystallizing clinopyroxene shows Mg# ≤ 70 (Fig. 4b) while in the equilibrium experiments of Masotta et al. (2010), plagioclase crystallizes cotectically with clinopyroxene when the latter shows Mg# ≤ 40.

The $^{87}Sr/^{86}Sr$ ratio of the Colli Albani magmas is relatively insensitive to the geochemical signal of the crustal contamination (i.e., highly radiogenic magmas emplaced in sedimentary carbonates) and, therefore, it defines a clear, relatively poorly scattered trend in the $^{87}Sr/^{86}Sr$ vs. time plot, with only rare out-trend samples showing lower isotopic values (Gaeta et al. 2016). For example, in the Pozzolane Rosse eruptive cycle from the Colli Albani (spanning 456 ± 3 to 441 ± 5 ka), the $^{87}Sr/^{86}Sr$ isotopic values decrease from 0.7106 for the main pyroclastic products to 0.7100 for the lava flow (Fig. 9). Conversely, over the same time window (i.e., the early Southern Sabatini; 461 ± 2 to 447 ± 7 ka time span), we observe the opposite trend (Fig. 9). In fact, $^{87}Sr/^{86}Sr$ isotopic values increase from 0.7104 (~ 461 ka Fall C) to 0.7111 (~ 447 ka Fall F). In particular, Fall F shows three clinopyroxene populations (Fig. 5), characterized by a wide range of textures and chemical compositions as a result of prolonged crystallization in the SVD plumbing system. The hosting juvenile pyroclasts represent, indeed, the fragmentation of a clinopyroxene-rich magma coming from a polybaric mush column (e.g., Tecchiato et al. 2018a, b). Accordingly, Fall F clinopyroxenes show the highest amount of $Al^{VI}$ (Fig. 10).

As a whole, the eruptive products that followed the Southern Sabatini activity display the widest isotopic variations (0.7095–0.7112). This is probably due to the contribution of carbonate rocks, as well as of Si-rich rocks, to the crustal contamination process of SVD magmas. Notably, the Sacrofano Caldera products show a narrow range of the $^{87}Sr/^{86}Sr$ ratios (Fig, 6b), quite similar to the coeval products of Colli Albani (Gaeta et al. 2006, 2009). Consistently, the Sacrofano Caldera products also show clear evidence of an interaction between magma and crustal carbonate rocks, as

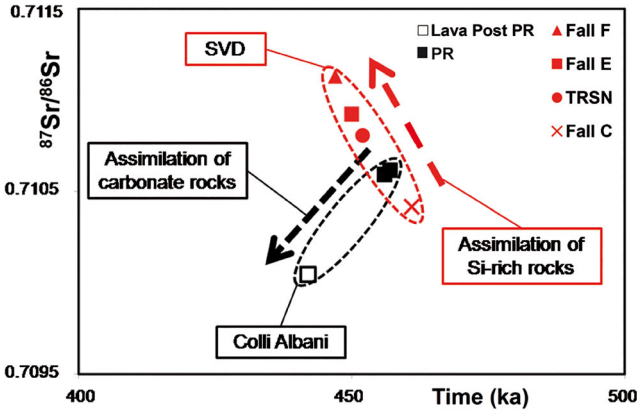


**Fig. 9** The $^{87}Sr/^{86}Sr$ vs time diagram highlights the different trends of coeval rocks of the SVD and Colli Albani. The SVD volcanic products from Fall C (~461 ka) to Fall F (~447 ka; i.e., late Southern Sabatini activity) show an increase of $^{87}Sr/^{86}Sr$ from 0.710416 to 0.711131, due to the assimilation of Si-rich rocks. Conversely, the Colli Albani volcanic products belonging to the Pozzolane Rosse eruptive cycle (456 ± 3 to 441 ± 5 ka) show a $^{87}Sr/^{86}Sr$ decrease from 0.710616 to 0.710046, due to the assimilation of sedimentary carbonate rocks

inferred from petrological and microtextural data (e.g., Facchinelli and Gaeta 1992).

## Remarks on the tephrostratigraphic implications

### General background

Although in the framework of the central Mediterranean tephrostratigraphy only a few studies applying Sr and Nd isotope compositions have been hitherto carried out (i.e., Roulleau et al. 2009; Giaccio et al. 2013a, 2013b, 2014; D'Antonio et al. 2016; Giaccio et al. 2015), these reveal the great potential of this method as an integrative tool for identifying the volcanic sources of distal tephra. The presented dataset here allows us to further test this approach and complete a critical review of all the literature study cases that report Sr-Nd isotope compositions and proposed possible correlations of distal tephra with Sabatini activity, on the basis of isotope composition and/or glass major element composition (e.g., Roulleau et al. 2009; Giaccio et al. 2014; Giaccio et al. 2015). These are from the Sulmona, Pianico Sellere, Mercure, and Fucino basins and are all lacustrine successions located in Central Apennine and southern Prealpine region (Fig. 1; Table 3).

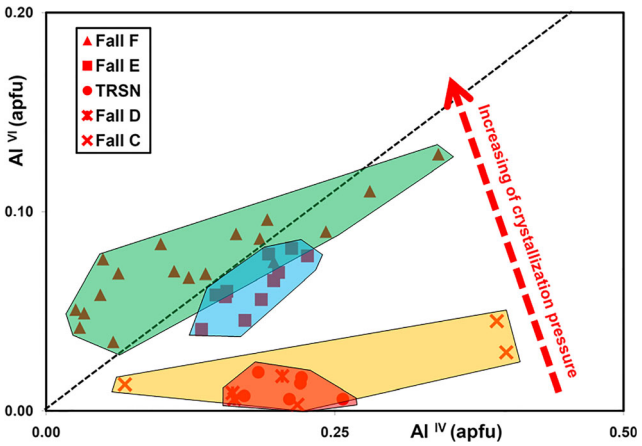


**Fig. 10** $Al^{IV}$ versus $Al^{VI}$ (atoms per formula unit, afu) of selected SVD clinopyroxenes. The dashed line that divides high- (above) and low (below)-pressure clinopyroxenes is based on literature experimental data from the LEPR (Library of Experimental Phase Relations) database (http://lepr.ofm-research.org/YUI/access_user/login.php)

### Distal tephra ascribable to the SVD paleo-activity

Seven distal tephra were stratigraphically ordered tephra, five of which have been directly dated by $^{40}Ar/^{39}Ar$ method between ~800 and ~720 ka (Giaccio et al. 2015). These tephra are from the lacustrine succession of Sulmona unit 6, which yielded high-resolution records of the paleohydrological variability over the marine isotope stage (MIS) 20–18 (Table 3; Giaccio et al. 2015) and of the Matuyama–Brunhes geomagnetic reversal (e.g., Sagnotti et al. 2016). Sr isotopes of bulk samples of the layers SUL2-25, SUL2-10, and SUL2-4 are in the range of those measured by us on products from the SVD Paleo-activity (i.e., ~0.711), while SUL2-7, SUL2-15, SUL2-16, and SUL2-22 yielded a slightly lower value of ~0.7109–0.7108 (Giaccio et al. 2015). These values might reflect either a primary geochemical signature—ascribable to different volcanic sources or isotopic variability/disequilibrium within products from the same eruptive period/eruption—or a secondary isotopic shift of the glass component due to weathering. The correct evaluation of the origin of the isotopic signature of volcanic products is fundamental in geochemical as well as in tephrostratigraphic studies, as recently shown by Giaccio et al. (2013b). In fact, due to weathering processes and/or to the isotopic variability of the erupted products, $^{87}Sr/^{86}Sr$ compositions of the bulk samples can yield slightly lower or higher values than those measured on pristine components (e.g., clinopyroxene crystals or fresh glass) from the same tephra, thus highlighting the need to analyze unaltered materials. However, although we cannot definitely assess that the isotopic signature of the SUL2-7, SUL2-15, SUL2-16, and SUL2-22 tephra is a primary feature of these products, the strong affinity of the major element compositions of the glass from these seven tephra (Giaccio et al. 2013a) suggests a common volcanic origin, which can be now restricted to the SVD paleo-activity. Furthermore, the $^{40}Ar/^{39}Ar$ ages of SUL2-25, SUL2-16, and SUL2-10 obtained from Giaccio et al. (2013a) spanning 802 ± 2–749 ± 2 ka (Table 3) overlap those of the SVD paleo-activity of 808 ± 6–763 ± 8 ka investigated here (Table 1).

Another distal tephra isotopically consistent with the SVD paleo-activity occurs in Pianico Sellere lacustrine succession (Roulleau et al. 2009), northern Italy (Fig. 1). Although this layer (t32) was previously attributed to a younger (~400 ka) activity of Roccamonfina volcano (Brauer et al. 2007),

**Table 3** Available $^{87}Sr/^{86}Sr$ analyses and associated $^{40}Ar/^{39}Ar$ on distal ash layers attributed to the Sabatini Volcanic District activity. All reported $^{87}Sr/^{86}Sr$ data refer to bulk analyses. References: 1—Giaccio et al. (2014); 2—Roulleau et al. (2009); 3—Giaccio et al. (2013a) and reference therein; 4—Giaccio et al. (2015). All $^{40}Ar/^{39}Ar$ ages re-calculated here for Alder Creek sanidine at 1.186 Ma

| Locality | Sample | Lat. (N) | Long. (E) | Rock types | $^{87}Sr/^{86}Sr$ | $\pm 2\sigma \times 10^{-6}$ | $^{40}Ar/^{39}Ar$ age (ka $\pm 2\sigma$) | Ref. |
|---|---|---|---|---|---|---|---|---|
| Mercure basin | SC3 | 39°57′ 12″ | 16°03′04″ | P | 0.711115 | 7 | > 489 ± 21<br>< 513 ± 5 | 1 |
| Pianico Sellere | t-32 | 45°48′ 45″ | 10°20′58″ | Tp-P | 0.711031 | 18 | > 779 ± 13 ka[a] | 2 |
| Sulmona basin | SUL1-1 | 42°10′ | 13°49′10″ | Te | 0.710441 | 10 | > 453 ± 1 | 3, 4 |
| | SUL1-2 | 26″ | | Te | 0.710540 | 14 | < 718.9 ± 1.6 | |
| | SUL1-3 | | | Tp-P | 0.710437 | 6 | | |
| | SUL1-4 | | | Te | 0.709967 | 7 | | |
| | SUL2-4 | 42°09′ 01″ | 13°49′03″ | P | 0.711094 | 11 | > 718.9 ± 1.6<br>< 743.7 ± 2.6 | |
| | SUL2-7 | 42°09′ | 13°48′58″ | Tp-P | 0.710977 | 6 | 743.7 ± 2.6 | |
| | SUL2-10 | 08″ | | Pte-Te | 0.711022 | 7 | 749.4 ± 1.7 | |
| | SUL2-15 | 42°09′ 38″ | 13°49′25″ | P | 0.710907 | 9 | 767.6 ± 1.6 | |
| | SUL2-16 | 42°09′ 04″ | 13°49′17″ | Tp-P | 0.710821 | 5 | 776.3 ± 2.0 | |
| | SUL2-22 | 42°09′ | 13°48′49″ | P | 0.710837 | 7 | 785.9 ± 1.9 | |
| | SUL2-25 | 06″ | | Tp-P | 0.711150 | 9 | > 785.9 ± 1.9 < 801.7 ± 2.3 | |

$SC^{143}Nd/^{144}Nd = 0.512110 \pm 0.000006$

Rock type: *P* phonolite, *Tp* tephriphonolite, *Te* tephrite, *Pte* phonotephrite

[a] K-Ar dating

magnetostratigraphic data, indicating that the succession encompasses the Matuyama–Brunhes geomagnetic reversal (Scardia and Muttoni 2009) and the K–Ar radiometric age of the underlying tephra t21 (779 ± 13 ka; Pinti et al. 2001), consistently suggest an age within the MIS 19 or the early Brunhes Chron, i.e., coeval to both SVD paleo-activity and tephra from Sulmona 6 unit. Specifically, $^{87}Sr/^{86}Sr$ and $^{143}Nd/^{144}Nd$ isotope ratios of the layer t32 determined by Roulleau et al. (2009) are 0.711031 and 0.512198, respectively, which allowed authors to attribute it to the early activity of SVD. This Sr isotope composition is well in the range of those measured by us for the volcanic products erupted during the SVD activity, while $^{143}Nd/^{144}Nd$ ratio is too high with respect to all volcanic products from the Colli Albani Volcanic District (Boari et al. 2009; Gaeta et al. 2016) and the SVD (Del Bello et al. 2014; this paper). In general, Sr–Nd composition of t32 is beyond the compositional field of the Quaternary potassic series of Italy (e.g., Peccerillo 2001). Indeed, Roulleau et al. (2009) report that Nd standard JNdi yielded a value of $^{143}Nd/^{144}Nd$ (0.512148), significantly "lower" than the value of 0.512115 given by Tanaka et al. (2000), and that they corrected the measured Tephra t32 Nd ratio using the offset of 0.000033. A close look at the previously reported values suggests that the JNdi standard yielded a value of $^{143}Nd/^{144}Nd$ higher than the published value (0.512115; Tanaka et al. 2000). The anomalous Nd isotope composition of t32 can be explained by assuming a wrong correction of the measured isotope ratio with respect to the JNdi standard (see "Methods" in Roulleau et al. 2009). In fact, by subtracting the offsets to the measured ratio, it is possible to obtain a $^{143}Nd/^{144}Nd$ ratio of 0.512132, i.e., within the errors of those obtained by us for products from the SVD paleo-activity.

Furthermore, the chemical composition of the glass type "a" from tephra t32, which is the most abundant (80%) among the three types of glass characterizing this ash layer (Roulleau et al. 2009), matches the major element composition of the layer SUL2-11, to which t32 can be thus tentatively correlated (Fig. 11). Therefore, by inference, also the layer SUL2-11, for which no Sr–Nd isotope data are available, can be attributed to the SVD paleo-activity. The correlation of layer SUL2-11/t32 to the SVD paleo-activity is further supported by the major element composition of these samples that is similar to that of the layer SUL2-10, which in turn is isotopically and chronologically compatible with the Ponte Galeria Eruptive Unit of the SVD paleo-activity phase. Finally, from a chronological point of view, according to the Bayesian age model for Sulmona MIS 19 record (Giaccio et al. 2015), the layer SUL2-11 can be dated to ~ 751.1 ± 2.7 ka, thus comparable to the $^{40}Ar/^{39}Ar$ age of Ponte Galeria Eruptive Unit (762.7 ± 8 ka).

### Fall A from Mercure Basin

A further isotopically characterized distal tephra from SVD has been found in the Mercure basin succession in southern Italy (Giaccio et al. 2014). This layer (SC3) was correlated via major element glass composition and $^{40}Ar/^{39}Ar$ chronological constraints to the Fall A Unit, which recently has been traced in a number of distal records, including the Eastern Sabatini area, Acerno and Sulmona Apennine intermountain basins, the

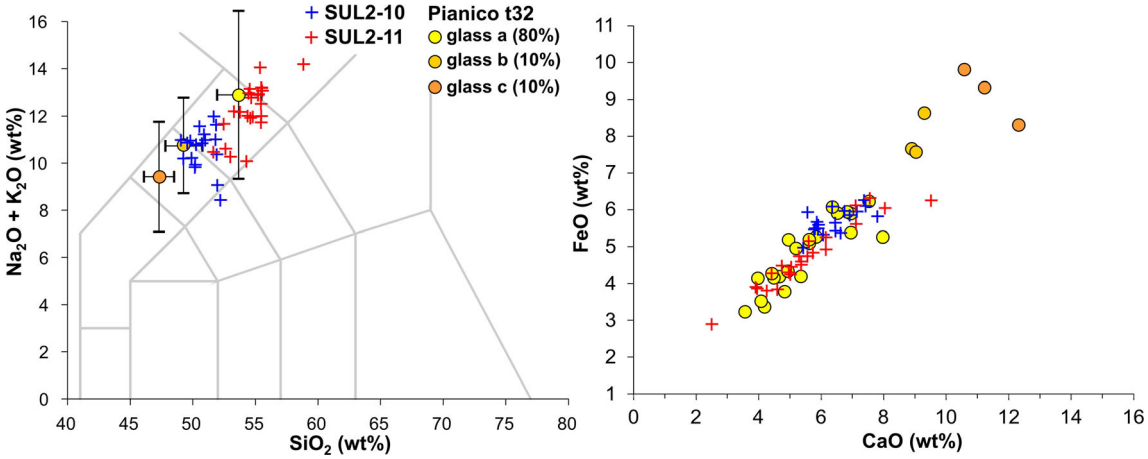


**Fig. 11** Total alkali versus silica classification diagram with a representative bi-plot (CaO and FeO wt% from glass compositions) showing the correlation between t-32 from the Pianico Sellere succession (Roulleau et al. 2009) and the SUL2-11 tephra from the Sulmona basin (Giaccio et al. 2013a and reference therein). For comparison, the composition of the glass from the SUL2-10 tephra is also shown (Giaccio et al. 2013a). Horizontal and vertical bars in the TAS diagram are the standard deviation of the mean, as reported in Roulleau et al. (2009)

Tyrrhenian marginal basin of Tarquinia of central Italy, and lake Ohrid in the Balkan area (Petrosino et al. 2014; Giaccio et al. 2014, Aureli et al. 2015; Leicher et al. 2015; Di Rita and Sottili 2019). $^{87}Sr/^{86}Sr$ and $^{143}Nd/^{144}Nd$ of a bulk sample of layer SC3 yielded values of 0.71112 and 0.51211, with the former slightly less enriched in radiogenic Sr and the latter similar, within analytical errors, to the Fall A sample and in the range of the late Morlupo and Southern Sabatini phases (Table 1).

### SVD late activity traced Fucino Basin

We finish by considering layer TF-14 from the Fucino Basin lacustrine succession in central Italy (Giaccio et al. 2015). Layer TF-14 was ascribed (Giaccio et al. 2015) via glass major element composition and Sr–Nd isotope ratios to the SVD. $^{87}Sr/^{86}Sr$ and $^{143}Nd/^{144}Nd$ of layer TF-14 yielded 0.70978 and 0.51212, respectively, which are in the field of SVD (Giaccio et al. 2015). In light of our data, we can be more confident in proposing this attribution being the Sr and Nd isotope compositions of TF-14 very close to those obtained by us for the Baccano Lower Unit (0.70954 and 0.51214, respectively, Table 1). The TF-14 was also directly dated by $^{40}Ar/^{39}Ar$ method at 125.6 ± 1.0 ka (Giaccio et al. 2015), thus further confirming that it belongs to the late activity phase (150–90 ka) of the SVD.

## Conclusions

We provide a comprehensive chemical and isotopic (Sr and Nd) dataset for SVD clinopyroxenes from pyroclastic and lava units, thus obtaining a representative isotope characterization over the whole eruptive history of the district (0.8–0.07 Ma) in a well-constrained $^{40}Ar/^{39}Ar$ age frame. The measured $^{87}Sr/^{86}Sr$ ratio in clinopyroxene from the SVD ranges between 0.71150 and 0.70954, while the $^{143}Nd/^{144}Nd$ ratio spans between 0.51214 and 0.51209. We found that on a long-term time-scale, i.e., over the whole SVD eruptive history of 0.8–0.07 Ma, Sr and Nd isotope compositions gradually decrease, thus highlighting a time-dependent geochemical trend of the erupted magmas. We also observe that Sr isotope composition vary notably within each of the six eruptive phases, with the minimum and maximum extremes almost equaling the variation of the entire eruptive history. This suggest more complex geochemical evolution trajectories than those described at the nearby ultrapotassic Colli Albani (0.6–0.04 Ma). In fact, geochemical features of clinopyroxene in lavas and juvenile pyroclasts suggest a magmatic differentiation in the SVD plumbing system open to exchange with Si-bearing rocks rather than with carbonate rocks as for the Colli Albani case.

From a tephrostratigraphic point of view, the results of this study confirm the potential of the use of Sr–Nd isotope data as integrative tool, jointly with the more classic geochemical analysis, for tracing the volcanic source of distal tephra, circumscribing the specific volcano and eruptive period or even identifying the individual proximal correlative unit. In the context of the current literature for the Middle Pleistocene tephrostratigraphy in the central Mediterranean region, the presented dataset here may provide important isotopic constraints for enhancing the application of this integrated stratigraphic, geochronological, and petrographic method.

**Acknowledgments** We thank Andrea Marzoli and an anonymous reviewer for the helpful comments and the Associate Editor, Steve Self, and the Executive Editor, Andrew Harris, for the additional precious suggestions. The authors kindly thank Sonia Tonarini for her assistance in the Mass Spectrometry Laboratory of the Istituto Geoscienze e Georisorse-CNR, Pisa, Italy.

**Funding information** This research was partly funded by the project "Microtextural, petrological and geochemical analyses on pyroclastic products from the volcanic districts of the Colli Albani and the Sabatini Volcanic District aimed at developing predictive models of volcanic hazard" (responsible Gianluca Sottili), funded by Sapienza-Università di Roma (Year 2017).

## References

Aureli, D., Contardi, A., Giaccio, B., Jicha, B., Lemorini, C., Madonna, S., Magri, D., Marano, F., Milli, S., Modesti, V., Palombo, M.R., Rocca, R. 2015. Palaeoloxodon and human interaction: depositional setting, chronology and archaeology at the Middle Pleistocene Ficoncella site (Tarquinia, Italy) PLoS One, 10 (4), art. no. e0124498

Avanzinelli R, Lustrino M, Mattei M, Melluso L, Conticelli S (2009) Potassic and ultrapotassic magmatism in the circum-Tyrrhenian region: the role of carbonated pelitic vs. pelitic sediment recycling at destructive plate margin. Lithos 113:213–227

Barberi F, Buonasorte G, Cioni R, Fiordelisi A, Foresi L, Iaccarino S, Laurenzi MA, Sbrana A, Vernia L, Villa IM (1994) Plio-Pleistocene geological evolution of the geothermal area of Tuscany and Latium. Mem Descr Carta Geol It 49:77–134

Beccaluva L, Di Girolamo P, Serri G (1991) Petrogenesis and tectonic setting of the Roman volcanic province, Italy. Lithos 26:191–221

Brauer A, Wulf S, Mangili C, Moscariello A (2007) Tephrochronological dating of varved interglacial lake deposits from Piànico-Sèllere (Southern Alps, Italy) to around 400 ka. J Quat Sci 22:85–96

Bell K, Lavecchia G, Rosatelli G (2013) Cenozoic Italian magmatism: isotope constraints for possible plume-related activity. J S Am Earth Sci 41:22–40

Boari E, Avanzinelli R, Melluso L, Giordano G, Mattei M, De Benedetti A, Morra V, Conticelli S (2009) Isotope geochemistry (Sr–Nd–Pb) and petrogenesis of leucitebearing volcanic rocks from "Colli Albani" volcano, Roman Magmatic Province, Central Italy: inferences on volcano evolution and magma genesis. Bull Volcanol 71: 977–1005

Buttinelli M, de Rita D, Cremisini C, Cimarelli C (2011) Deep explosive focal depths during maar forming magmatic-hydrothermal eruption: Baccano crater, Central Italy. Bull Volcanol 73(7):899–915

Castorina F, Stoppa F, Cundari A, Barbieri M (2000) An enriched mantle source for Italy's melilitite-carbonatite association as inferred by its Nd-Sr isotope signature. Mineral Mag 64:625–639

Cioni R, Laurenzi MA, Sbrana A, Villa IM (1993) $^{40}Ar/^{39}Ar$ chronostratigraphy of the initial activity in the Sabatini volcanic complex (Italy). Boll Soc Geol It 112:251–263

Conticelli S, Peccerillo A (1992) Petrology and geochemistry of potassic and ultrapotassic volcanism in Central Italy: petrogenesis and inferences on the evolution of the mantle sources. Lithos 28:221–240

Conticelli S, Francalanci L, Manetti P, Cioni R, Sbrana A (1997) Petrology and geochemistry of the ultrapotassic rocks from the Sabatini volcanic district, Central Italy: the role of evolutionary processes in the genesis of variably enriched alkaline magmas. J Volcanol Geotherm Res 75:107–136

Conticelli S, D'Antonio M, Pinarelli L, Civetta L (2002) Source contamination and mantle heterogeneity in the genesis of Italian potassic and ultrapotassic volcanic rocks: Sr-Nd-Pb isotope data from Roman province and southern Tuscany. Mineral Petrol 74:189–222

Conticelli S, Avanzinelli R, Ammannati E, Casalini M (2015) The role of carbon from recycled sediments in the origin of ultrapotassic igneous rocks in the Central Mediterranean. Lithos 232:293–299

Conticelli S, Laurenzi MA, Giordano G, Mattei M, Avanzinelli R, Melluso L, Tommasini S, Boari E, Cifelli F, Perini G (2010) Leucite-bearing (kamafugitic/leucititic) and -free (lamproitic) ultrapotassic rocks and associated shoshonites from Italy: constraints on petrogenesis and geodynamics. In: Beltrando, M., Peccerillo, A., Mattei, M., Conticelli, S., Doglioni, C. (Eds.), Journal of the Virtual Explorer, volume 36, paper 20, https://doi.org/10.3809/jvirtex.2009.00251

Conticelli S, Marchionni S, Rosa D, Giordano G, Boari E, Avanzinelli R (2009) Shoshonite and sub-alkaline magmas from an ultrapotassic volcano: Sr–Nd–Pb isotope data on the Roccamonfina volcanic rocks. Roman Magmatic Province, Southern Italy Contributions to Mineralogy and Petrology, 157, pp. 41–63

Cross JK, Tomlinson EL, Giordano G, Smith VC, De Benedetti AA, Roberge J, Manning CJ, Wulf S, Menzies MA (2014) High level triggers for explosive mafic volcanism: Albano Maar, Italy. Lithos 190–191:137–153

D'Antonio M, Mariconte R, Arienzo I, Mazzeo FC, Carandente A, Perugini D, Petrelli M, Corselli C, Orsi G, Principato MS, Civetta L (2016) Combined Sr-Nd isotopic and geochemical fingerprinting as a tool for identifying tephra layers: application to deep-sea cores from eastern Mediterranean Sea. Chem Geol 443:121–136

Dallai L, Freda C, Gaeta M (2004) Oxygen isotope geochemistry of pyroclastic clinopyroxene monitors carbonate contributions to Roman-type ultrapotassic magma. Contrib Mineral Petrol 148: 247–263

de Rita D, Funiciello R, Corda L, Sposato A, Rossi U (1993) Volcanic units. In: Di Filippo M (ed) Sabatini volcanic complex: quad, Ric. Sci, vol 114. Roma, Progetto Finalizzato Geodinamica C.N.R, pp 33–79

de Rita D, Di Filippo M, Rosa C (1996) Structural evolution of the Bracciano volcanotectonic depression, Sabatini Volcanic District, Italy. In: McGuire, W.J., Jones, A.P., Neuberg, J. (Eds.), Volcano instability on the Earth and other planets: Geol. Soc. London Spec. Publ., Vol. 110, 225–236

Di Rita F, Sottili G (2019) Pollen analysis and tephrochronology of a MIS 13 lacustrine succession from eastern Sabatini Volcanic District (Rignano Flaminio, Central Italy). Quat Sci Rev 204:78–93. https://doi.org/10.1016/j.quascirev.2018.11.027

Del Bello E, Mollo S, Scarlato P, von Quadt A, Forni F, Bachmann O (2014) New petrological constraints on the last eruptive phase of the Sabatini Volcanic District (Central Italy): clues from mineralogy, geochemistry, and Sr-Nd isotopes. Lithos 205:28–38

Di Rocco T, Freda C, Gaeta M, Mollo S, Dallai L (2012) Magma chambers emplaced in carbonate substrate: petrogenesis of skarn and cumulate rocks and implication on $CO_2$-degassing in volcanic areas. J Petrol 53:2307–2332

Facchinelli V, Gaeta M (1992) Petrogenetic implications from birefringent garnets in the sialic ejecta in the alkaline-potassic volcanics of Sabatini Mts. (Latium, Italy). [Indicazioni petrogenetiche dai granati birifrangenti dei proietti sialici nelle vulcaniti alcalino potassiche dei Monti Sabatini (Lazio)] Rendiconti Lincei 3(4):295–310

Florindo F, Karner DB, Marra F, Renne PR, Roberts AP, Weaver R (2007) Radioisotopic age constraints for glacial terminations IX and VII from aggradational sections of the Tiber River delta in Rome. Italy Earth Planet Sci Lett 256:61–80

Freda C, Gaeta M, Palladino DM, Trigila R (1997) The Villa Senni eruption (Alban Hills, Central Italy): the role of H2O and CO2 on the magma chamber evolution and on the eruptive scenario. J Volcanol Geotherm Res 78:103–120

Gaeta M, Freda C (2001) Strontian fluoro-magnesiohastingsite in Alban Hills lavas (Central Italy): crystallization conditions. Mineralogical Magazine 65:787–795

Gaeta M, Palladino DM, Karner DB, Renne PR (2003) Vulcanoclastiti della Valle del Corno (vvc). Note Illustrative della Carta Geologica d'Italia alla scala 1:50.000-foglio 358 Pescorocchiano. Regione Lazio, pp. 34–35. A cura di Centamore E., Dramis F Rome, in press

Gaeta M, Freda C, Christensen JN, Dallai L, Marra F, Karner DB, Scarlato P (2006) Time-dependent geochemistry of clinopyroxene from the Alban Hills (Central Italy): clues to the source and evolution of ultrapotassic magmas. Lithos 86(3–4):330–346

Gaeta M, Di Rocco T, Freda C (2009) Carbonate assimilation in open magmatic systems: the role of melt-bearing skarns and cumulate-forming processes. J Petrol 50:361–385

Gaeta M, Freda C, Marra F, Di Rocco T, Gozzi F, Arienzo I, Giaccio B, Scarlato P (2011) Petrology of the most recent ultrapotassic magmas from the Roman province (Central Italy). Lithos 127:298–308

Gaeta M, Freda C, Marra F, Arienzo I, Gozzi F, Jicha B, Di Rocco T (2016) Paleozoic metasomatism at the origin of Mediterranean ultrapotassic magmas: constraints from time-dependent geochemistry of Colli Albani volcanic products (Central Italy). Lithos 244: 151–164

Gasperini D, Blichert Toft J, Bosch D, Del Moro A, Macera P, Albaréde F (2002) Upwelling of deep mantle material through a plate window: evidence from the geochemistry of Italian basaltic volcanics. J Geophys Res 107(B12):2367–ECV 7-19. https://doi.org/10.1029/2001JB000418

Giaccio B, Messina P, Sposato A, Voltaggio M, Zanchetta G, Galadini F, Gori S, Santacroce R (2009) Tephra layers from Holocene lake sediments of the Sulmona Basin, Central Italy: implications for volcanic activity in peninsular Italy and tephrostratigraphy in the Central Mediterranean area. Quat Sci Rev 28(25–26):2710–2733

Giaccio B, Castorina F, Nomade S, Scardia G, Voltaggio M, Sagnotti L (2013a) Revised chronology of the Sulmona lacustrine succession, Central Italy. J Quat Sci 28(6):545–551

Giaccio B, Arienzo I, Sottili G, Castorina F, Gaeta M, Nomade S, Galli P, Messina P (2013b) Isotopic (Sr-Nd) and major element fingerprinting of distal tephras: an application to the Middle-Late Pleistocene markers from the Colli Albani volcano, Central Italy. Quat Sci Rev 67:190–206

Giaccio B, Galli P, Peronace E, Arienzo I, Nomade S, Cavinato GP, Mancini M, Messina P, Sottili G (2014) A 560-440 ka tephra record from the Mercure Basin, southern Italy: volcanological and tephrostratigraphic implications. J Quat Sci 29(3):232–248

Giaccio B, Regattieri E, Zanchetta G, Nomade S, Renne PR, Sprain CJ, Drysdale RN, Tzedakis PC, Messina P, Scardia G, Sposato A, Bassinot F (2015) Duration and dynamics of the best orbital analogue to the present interglacial. Geology 43(7):603–606

Goldstein SL, Deines P, Oelkers EH, Rudnick RL, Walter LM (2003) Standards for publication of isotope ratio and chemical data in chemical geology. Chem Geol 202:1–4

Gozzi F, Gaeta M, Freda C, Mollo S, Di Rocco T, Marra F, Dallai L, Pack A (2014) Primary magmatic calcite reveals origin from crustal carbonate. Lithos 190–191:191–203

Hawkesworth CJ, Vollmer R (1979) Crustal contamination vs. enriched mantle: $^{143}Nd/^{144}Nd$ and $^{87}Sr/^{86}Sr$ evidence from the Italian volcanics. Contrib Mineral Petrol 69:151–165

Iacono Marziano G, Gaillard F, Pichavant M (2007) Limestone assimilation and the origin of CO2 emission at the Alban Hills (Central Italy): constraints from experimental petrology. J Volcanol Geotherm Res 166:91–105

Jicha BR, Singer BS, Sobol P (2016) Re-evaluation of the ages of 40Ar/39Ar sanidine standards and supereruptions in the western U.S. using a noblesse multi-collector mass spectrometer. Chem Geol 431:54–66

Karner DB, Marra F (1998) Correlation of fluviodeltaic aggradational sections with glacial climate history: a revision of the classical Pleistocene stratigraphy of Rome. Geol Soc Am Bull 110:748–758

Karner DB, Renne PR (1998) $^{40}Ar/^{39}Ar$ geochronology of Roman province tephra in the Tiber River valley: age calibration of middle Pleistocene sea-level changes. Geol Soc Am Bull 110:740–747

Karner DB, Marra F, Renne P (2001) The history of the Monti Sabatini and Alban Hills volcanoes: groundwork for assessing volcanic-tectonic hazards for Rome. J Volcanol Geotherm Res 107:185–219

Kuiper KF, Deino A, Hilgen FJ, Krijgsman W, Renne PF, Wijbrans JR (2008) Synchronizing rock clocks of earth history. Science 320: 500e504–500e504. https://doi.org/10.1126/science.1154339

Laurora A, Malferrari D, Brigatti MF, Mottana A, Caprilli E, Giordano G, Funiciello R (2009) Crystal chemistry of trioctahedral micas in the top sequences of the Colli Albani volcano, Roman region, Central Italy. Lithos 113:507–520

Laurenzi MA, Villa IM (1987) $^{40}Ar/^{39}Ar$ chronostratigraphy of the Vico ignimbrites. Per Mineral 56:285–293

Laurenzi M, Braschi E, Casalini M, Conticelli S (2015) New $^{40}Ar–^{39}Ar$ dating and revision of the geochronology of the Monte Amiata volcano, Central Italy. Ital J Geosci 134:255–265

Le Bas MJ, Le Maitre RW, Streckeisen A, Zanettin B (1986) A chemical classification of volcanic rocks based on the total alkali–silica diagram. J Petrol 27:745–750

Leicher N, Zanchetta G, Sulpizio R, Giaccio B, Wagner B, Nomade S, Francke A, Del Carlo P (2015) First tephrostratigraphic results of the DEEP site record from Lake Ohrid. Macedonia Biogeosciences Discuss 12:15411–15460. https://doi.org/10.5194/bgd-12-15411-2015

Marra F, Florindo F (2014) The subsurface geology of Rome: sedimentary processes, sea-level changes and astronomical forcing. Earth Sci Rev 136:1–20

Marra F, Sottili G, Gaeta M, Giaccio B, Jicha B, Masotta M, Palladino DM, Deocampo DM (2014) Major explosive activity in the Monti Sabatini Volcanic District (Central Italy) over the 800-390ka interval: geochronological-geochemical overview and tephrostratigraphic implications. Quat Sci Rev 94:74–101

Marra F, Jicha B, Florindo F (2017) 40Ar/39Ar dating of glacial termination VI: constraints to the duration of marine isotopic stage 13. Sci Rep 7:8908. https://doi.org/10.1038/s41598-017-08614-6

Marra F, Florindo F, Jicha B, Nomade S, Palladino D, Pereira A, Sottili G, Tolomei C (2019) Assessing volcano-tectonic hazard of the Monti Sabatini Volcanic District on the city of Rome (central Italy): evidence from new geochronologic constraints on the Tiber River MIS 5 terraces. Sci Rep 9:11496. https://doi.org/10.1038/s41598-019-47585-8

Masotta M, Gaeta M, Gozzi F, Marra F, Palladino DM, Sottili G (2010) $H_2O$- and temperature-zoning in magma chambers: the example of the Tufo Giallo della via Tiberina eruptions (Sabatini Volcanic District, Central Italy). Lithos 118:119–130

Mazzeo FC, D'Antonio M, Arienzo I, Aulinas M, Di Renzo V, Gimeno D (2014) Subduction-related enrichment of the Neapolitan volcanoes (southern Italy) mantle source: new constraints on the characteristics of the slab-derived components. Chem Geol 386:165–183

Morimoto N (1988) Nomenclature of pyroxenes. Mineral Petrol 39(1): 55–76

Mollo S, Gaeta M, Freda C, Di Rocco T, Misiti V, Scarlato P (2010) Carbonate assimilation in magmas: a reappraisal based on experimental petrology. Lithos 114:503–514

Nappi G, Mattioli M (2003) Evolution of the Sabatinian Volcanic District (Central Italy) as inferred by stratigraphic successions of its northern sector and geochronological data. Per Mineral 72:79–102

Palladino DM, Gaeta M, Giaccio B, Sottili G (2014) On the anatomy of magma chamber and caldera collapse: the example of trachyphonolitic explosive eruptions of the Roman province (Central Italy). J Volcanol Geotherm Res 281:12–26

Palladino DM, Valentine GA, Sottili G, Taddeucci J (2015) Maars to calderas: end-members on a spectrum of explosive volcanic depressions. Front Earth Sci 3:36. https://doi.org/10.3389/feart.2015.00036

Peccerillo A (1985) Roman Comagmatic Province (Central Italy): evidence for subduction-related magma genesis. Geology 13:103–106

Peccerillo A (1999) Multiple mantle metasomatism in Central-Southern Italy: geochemical effects, timing and geodynamic implications. Geology 27:315–318

Peccerillo A (2001) Geochemistry and petrogenesis of quaternary magmatism in Central-Southern Italy. Geochem Int 6:579–592

Peccerillo A, Frezzotti ML (2015) Magmatism, mantle evolution and geodynamics at the converging plate margins of Italy. J Geol Soc 172:407–427. https://doi.org/10.1144/jgs2014-085

Pereira A, Nomade S, Falguères C, Bahain J-J, Tombret O, Garcia T, Voinchet P, Bulgarelli AG, Anzidei P (2017) 40Ar/39Ar and ESR/U-series data for the La Polledrara di Cecanibbio archaeological site (Lazio, Italy). J Archaeol Sci Rep 15:20–29

Perini G, Francalanci L, Davidson JP, Ponticelli S (2004) Evolution and genesis of magmas from Vico volcano, Central Italy: multiple differentiation pathways and variable parental magmas. J Petrol 45: 139–182

Petrosino P, Jicha BR, Mazzeo FC, Russo Ermolli E (2014) A high resolution tephrochronological record of MIS 14-12 in the southern Apennines (Acerno Basin, Italy). J Volcanol Geotherm Res 274:34–50

Pinti DL, Quidelleur X, Chiesa S, Ravazzi C, Gillot PY (2001) K–Ar dating of an early middle Pleistocene distal tephra in the interglacial varved succession of Pianico-Sellere (southern Alps, Italy). Earth Planet Sci Lett 188:1–7

Roulleau E, Pinti DL, Rouchon V, Quidelleur X, Gillot P-Y (2009) Tephro-chronostratigraphy of the lacustrine interglacial record of Pianico, Italian southern Alps: identifying the volcanic sources using radiogenic isotopes and trace elements. Quat Int 204(1–2): 31–43

Renne PR, Balco G, Ludwig KR, Mundil R, Min K (2011) Response to the comment by W.H. Schwarz et al. on "joint determination of $^{40}K$ decay constants and $^{40}Ar^*/^{40}K$ for the fish canyon sanidine standard, and improved accuracy for $^{40}Ar/^{39}Ar$ geochronology" by P.R. Renne et al. (2010). Geochim Cosmochim Acta 75:5097–5100. https://doi.org/10.1016/j.gca.2011.06.021

Rivera TA, Storey M, Schmitz MD, Crowley JL (2013) Age intercalibration of $^{40}Ar/^{39}Ar$ sanidine and chemically distinct U/Pb zircon populations from the Alder Creek rhyolite quaternary geochronology standard. Chem Geol 345:87–98

Sagnotti L, Giaccio B, Liddicoat JC, Nomade S, Renne PR, Scardia G, Sprain CJ (2016) How fast was the Matuyama-Brunhes geomagnetic reversal? A new subcentennial record from the Sulmona Basin, Central Italy. Geophys J Int 204(2):798–812

Scardia G, Muttoni G (2009) Paleomagnetic investigations on the Pleistocene lacustrine sequence of Piànico-Sèllere (northern Italy). Quat Int 204(1–2):44–53

Sottili G, Palladino DM, Zanon V (2004) Plinian activity during the early eruptive history of the Sabatini Volcanic District, Central Italy. J Volcanol Geotherm Res 135:361–379

Sottili G, Palladino DM, Marra F, Jicha B, Karner DB, Renne P (2010a) Geochronology of the most recent activity in the Sabatini Volcanic District, Roman province, Central Italy. J Volcanol Geotherm Res 196:20–30

Sottili G, Taddeucci J, Palladino DM (2010b) Constraints on magma-wall rock thermal interaction during explosive eruptions from textural analysis of cored bombs. J Volcanol Geoth Res 192(1–2):27–34

Sottili G, Palladino DM, Gaeta M, Masotta M (2012) Origins and energetics of maar volcanoes: examples from the ultrapotassic Sabatini Volcanic District (Roman province, Central Italy). Bull Volcanol 74: 163–186

Tanaka T, Togashi S, Kamioka H, Amakawa H, Kagami H, Hamamoto T, Yuhara M, Orihashi Y, Yoneda S, Shimizu H, Kunimaru T, Takahashi K, Yanagi T, Nakano T, Fujimaki H, Shinjo R, Asahara Y, Tanimizu M, Dragusanu C (2000) JNdi-1: a neodymium isotopic reference in consistency with LaJolla neodymium. Chem Geol 168(3–4):279–281

Tecchiato V, Gaeta M, Mollo S, Scarlato P, Bachmann O, Perinelli C (2018a) Petrological constraints on the high-Mg basalts from Capo Marargiu (Sardinia, Italy): evidence of cryptic amphibole fractionation in polybaric environments. J Volcanol Geotherm Res 349:31–46

Tecchiato V, Gaeta M, Mollo S, Bachmann O, von Quadt A, Scarlato P (2018b) Snapshots of primitive arc magma evolution recorded by clinopyroxene textural and compositional variations: the case of hybrid crystal-rich enclaves from Capo Marargiu Volcanic District (Sardinia, Italy). Am Mineral 103:899–910

Thirlwall MF (1991) Long-term reproducibility of multicollector Sr and Nd isotope ratio analysis. Chem Geol 94:85–104

Valentine GA, Sottili G, Palladino DM, Taddeucci J (2015) Tephra ring interpretation in light of evolving maar-diatreme concepts: Stracciacappa maar (Central Italy). J Volcanol Geotherm Res 308: 19–29

Washington HS (1906). The roman comagmatic region. Carnegie Institute Year Book 56:206–214